

Measurement Report: Optical Characterization, Seasonality, and Sources of Brown Carbon in Fine Aerosols from Tianjin, North China: Year-round Observations

Zhichao Dong¹, Chandra Mouli Pavuluri^{1*}, Peisen Li¹, Zhanjie Xu¹, Junjun Deng¹, Xueyan Zhao¹, Xiaomai Zhao¹, Pingqing Fu¹, Cong-Qiang Liu¹

¹Institute of Surface-Earth System Science, School of Earth System Science, Tianjin University, Tianjin 300072, China

Correspondence to: Chandra Mouli Pavuluri (cmpavuluri@tju.edu.cn)

Abstract

To investigate the optical characteristics and sources of brown carbon (BrC) in North China, where the atmospheric aerosol loadings are high and have severe impacts on the Earth's climate system, we collected fine aerosols (PM_{2.5}) at an urban site in Tianjin over a 1-year period. We measured the ultraviolet (UV) light absorption and excitation emission matrix (EEM) fluorescence of the water-soluble BrC (WSBrC) and the water-insoluble but methanol-soluble BrC (WI-MSBrC) in the PM_{2.5} using a three-dimensional fluorescence spectrometer. Average light absorption efficiency of both WSBrC ($Abs_{365, WSBrC}$) and WI-MSBrC ($Abs_{365, WI-MSBrC}$) at 365 nm was found to be highest in winter ($10.4 \pm 6.76 \text{ Mm}^{-1}$ and $10.0 \pm 5.13 \text{ Mm}^{-1}$, respectively) and distinct from season to season. Averages of fluorescence index (FI) and biological index (BIX) of WSBrC were lower in summer than in other seasons and opposite to that of humification index (HIX), which implied that the secondary formation and further chemical processing of aerosols were intensive during the summer period than in other seasons. Whereas in winter, the higher HIX together with the higher FI and BIX of WI-MSBrC suggested that the BrC loading was mainly influenced by primary emissions from biomass burning and coal combustion. Based on EEM, the types of fluorophores in WSBrC were divided into humic-like substances (HULIS), including low-oxygenated and high-oxygenated species, and protein like compounds (PLOM), whereas mostly PLOM in the WI-MSBrC. The direct radiation absorption by both WSBrC and WI-MSBrC in the range of 300–400 nm was accounted for ~40% to that (SFE, $4.97 \pm 2.71 \text{ Wg}^{-1}$ and $7.58 \pm 5.75 \text{ Wg}^{-1}$, respectively) in the range, 300–700 nm.

1 Introduction

Brown carbon (BrC) is a part of organic aerosol (OA) and can absorb solar radiation in the near-ultraviolet (UV) to visible (Vis) light, ranging from 300–500 nm (Liu et al., 2013). It has been well recognized that BrC has a significant effect on radiative forcing at both regional and global scales (Feng et al., 2013; Jo et al., 2016; Park et al., 2010). *For example*, the warming effect of water-soluble BrC in the Arctic has been reported to be accounted for ~30% of that exerted by the black carbon (Yue et al., 2022). The BrC not only affects the direct radiative forcing, but also has a potential impact on indirect radiative forcing due to its hydrophilicity, which influences the formation of cloud condensation nuclei (CCN) (Andreae and Gelencsér, 2006; Laskin et al., 2015a). In addition, BrC is mostly composed of highly conjugated aromatic ring compounds such

1 as a polycyclic aromatic hydrocarbons and high molecular weight substances with a polar
2 functional group that consists of nitrogen and/or oxygen, or humic-like substances (HULIS), which
3 could pose a risk to human health. *For example*, carbon-containing aromatic compounds can cause
4 physical weakness, decreased immunity, arteriosclerosis, etc., which will increase the mortality
5 due to cardiovascular and cerebrovascular diseases and a variety of cancers such as skin cancer,
6 pharyngeal cancer and nasal cancer (Diggs et al., 2011; Peters et al., 2008; Hecobian et al., 2010).

7 BrC can be emitted directly from primary sources such as biomass burning (Hoffer et al.,
8 2006; Brown et al., 2021), fossil fuel combustion (Jo et al., 2016), and non-combustion processes
9 such as bioaerosols (plant debris and fungi) and soil humus (Lin et al., 2014; Rizzo et al., 2013;
10 Rizzo et al., 2011). On the other hand, BrC can also be produced from complex chemical reactions
11 of volatile organic compounds (VOCs) emitted from both anthropogenic and biological origin in
12 gas-phase as well as by multiphase reactions between the gaseous, particulate and aqueous
13 constituents (Kasthuriarachchi et al., 2020; Li et al., 2020a; Laskin et al., 2015b).

14 In recent times, after establishing the fact that BrC absorb the light, the researchers are paying
15 lot of attention to measure the physical (optical) and chemical characteristics of the BrC and
16 estimate its climatic effects (Yue et al., 2019; Choudhary et al., 2021; Hecobian et al., 2010).
17 However, studies on BrC are still very limited due to difficulties in quantitative measurement of
18 light-absorbing organic components (Corbin et al., 2019; Wang et al., 2022b). In fact, based on
19 the disparity in wavelength dependence between BC and BrC, traditional optical instruments can
20 be used to obtain the BrC absorption value, but the availability of such instruments are limited,
21 which can accurately and directly differentiate the light absorption caused by the BC and BrC. On
22 the other hand, the molecular composition and optical properties of BrC are significantly changed
23 when the BrC is subjected for physical and photo-chemical processing (aging) in the atmosphere.
24 That is why, the indirect approaches have been developed to explore the molecular composition
25 including chromophores and sources of BrC through its light absorption and fluorescence
26 characteristics.

27 Ultraviolet-visible (UV-Vis) spectroscopy and excitation emission matrix (EEM)
28 fluorescence spectroscopy are considered to be common techniques for studying the optical
29 absorption and fluorescence chromophore optical and structural characteristics of complex organic
30 materials, because each chromophore has its own specific excitation-emission peak in the EEM
31 maps (Chen et al., 2016b; Coble, 2007). In recent years, combined spectrophotometric
32 measurement and chemical analysis has been applied to study the BrC in Xi'an, Northwest China
33 (Huang et al., 2018). In fact, EEM fluorescence spectroscopy provides multiple superposed
34 spectral data. By using parallel factor (PARAFAC) analysis of such spectral data, the type of
35 chromophores can be identified and their types are quantified semi-quantitatively based on the
36 range of excitation-emission wavelengths (Cao et al., 2022; Zhan et al., 2022; Murphy et al., 2013).
37 The composition of humic-like and protein-like components have been identified from the analysis
38 of chromophores of dissolved organic substances in aquatic environments (Xie et al., 2020). The
39 fluorescence technique has been widely applied to measure organics in terrestrial and oceanic
40 systems (Murphy et al., 2013; Yu et al., 2015), but has rarely been used in the study of atmospheric
41 aerosols. Now, the application of fluorescence technique has been well established in studying the
42 molecular composition of aerosols as well, the studies on identification of chromophores and thus
43 the molecular composition of BrC in the atmospheric aerosols are still very limited (Wu et al.,
44 2021a; Deng et al., 2022; Li et al., 2022; Cao et al., 2022).

45 Therefore, much attention need to be paid further, particularly on long-term and continuous
46 measurements of the optical characteristics of water-soluble BrC (WSBrC) and their temporal and

1 spatial variations. Moreover, the investigation of light absorption and fluorescence characteristics
2 of water-insoluble BrC (WIBrC) that can be extracted into a solvent with higher extraction
3 efficiency is necessary to better understand the impact of the BrC on climate change (Corbin et al.,
4 2019). In fact, such studies are very scarce, because the selection of solvents and determination of
5 extraction efficiency are difficult, although different polar chromophores could be extracted by
6 solvent extraction according to the polarity of solvent and methanol has been used as a common
7 solvent (Chen et al., 2016a). Hence, the comprehensive study of the optical properties of WSBrc
8 and WIBrC is highly necessary to better understand the types of chromophores and optical
9 properties of atmospheric aerosols, as well as the processes of oxidation and transformations of
10 chromophores at different locale over the world.

11 China is one of the most polluted areas in the world, and suffering from the absorption and
12 scattering of solar radiation by atmospheric aerosols that directly affect the energy balance of the
13 Earth's climate system, especially in North China Plain (Wang et al., 2022a). As an important port
14 city in the North China Plain, Tianjin, which has a large population, has received a widespread
15 attention to address the atmospheric environmental issues. Previous studies have shown that BrC
16 in the atmosphere contributes significantly to the light absorption by aerosols (Deng et al., 2022).
17 PM_{2.5} loading in the Tianjin area is extremely high, with greater abundance of organic matter (OM)
18 (Dong et al., 2023a). In such an environment, BrC is likely to become an important light-absorbing
19 component of atmospheric aerosols. However, the studies on physico-chemical characteristics and
20 sources of BrC are very limited in the North China Plain, and to the best of our knowledge, the
21 long-term observations of the optical properties and molecular composition of BrC have not been
22 reported yet over the Tianjin region.

23 In this study, we measured the optical properties and molecular composition of WSBrc and
24 water-insoluble but methanol-soluble BrC (WI-MSBrC) in fine aerosols (PM_{2.5}) collected from
25 Tianjin, North China over a one-year period using the combined UV-Vis absorption and EEM
26 fluorescence spectroscopy technique. We discussed the seasonal variations in optical properties
27 and chromophore composition of WSBrc and WI-MSBrC in the PM_{2.5}. We also assessed the
28 possible sources of BrC including the potential photochemical processing of OA (aging) over the
29 Tianjin region, based on the relationships between the BrC and chemical tracers and stable carbon
30 ($\delta^{13}\text{C}$) and nitrogen ($\delta^{15}\text{N}$) isotope ratios of total carbon (TC) and nitrogen (TN) in the PM_{2.5}. Thus,
31 this study provides a comprehensive understanding of the optical characteristics, seasonality, and
32 sources of BrC in the Tianjin region, and warrant the need to develop the prevention and control
33 strategies for the BrC and/or its precursors emissions.

34 **2 Materials and Methods**

35 **2.1 Aerosol sampling**

36 Fine aerosol (PM_{2.5}) sampling was conducted in Tianjin, a coastal city located at the lower
37 reaches of the Haihe River and Bohai Sea and 150 km away from Beijing in the northern part of
38 China. The sampling took place on the rooftop of a six-storey building at Tianjin University (ND,
39 39.11°N, 117.18°E) in an urban area of Nankai District, Tianjin. A high-volume air sampler (Tisch
40 Environmental, TE-6070DX) at a flow rate of 1.0 m³ min⁻¹ and pre-combusted (6 hours at 450°C)
41 quartz fiber filters (Pallflex 2500QAT-UP) were used for continuously collecting the PM_{2.5}
42 samples for 3 days (~72 hours) each during 5 July 2018 to 4 July 2019 ($n = 121$). Filter blanks
43 were collected twice per season during the campaign, following the same sampling procedure
44 placing the filter in hood for 10 mins without turning on the sampler pump.

1 Prior to and after sampling, each filter was dehumidified in a desiccator for 48 hours and
2 determined the PM_{2.5} mass by gravimetric analysis, and then stored in a pre-combusted glass jar
3 with a Teflon-lined cap in the dark at -20°C until analysis.

4 2.2 Measurement of carbonaceous and ionic components

5 Details of the measurements of aerosol organic carbon (OC), element carbon (EC) and water-
6 soluble organic carbon (WSOC) were described by Wang et al. (Wang et al., 2019) and Dong et
7 al. (Dong et al., 2023a). Briefly, concentrations of the OC and EC were measured using an aliquot
8 of filter (1.5. cm²) and a thermal-optical carbon analyzer (Sunset Laboratory Inc, USA), following
9 the IMPROVE protocol of the protective visual environment. WSOC was measured using an
10 aliquot of filter (one disc of either 14 mm or 22 mm in diameter) extracted into organic-free Milli
11 Q water and total organic carbon (TOC) analyzer (Model OI, 1030W + 1088). Concentrations of
12 K⁺ and Cl⁻ were determined using an aliquot of filter (one disc of 22 mm in diameter) extracted
13 into ultrapure water (>18.2MΩ cm) and ion chromatography (ICS-5000 System, China, Dai An)
14 (Dong et al., 2023a).

15 2.3 Measurement of optical properties of brown carbon (BrC)

16 2.3.1 Extraction and concentration of BrC

17 BrC was extracted into 30 ml ultrapure water using a sample filter disc of 22 mm in diameter
18 placed in a glass bottle with screw cap and sealed with Teflon tape under ultrasonication for 30
19 min. The extracts were filtered through a 0.45 μm polytetrafluoron (PTFE) syringe filter to remove
20 the water-insoluble particles and filter debris, and transferred into a clean glass bottle. The extracts
21 were used for the light absorption and fluorescence measurements of WSBrC. While the
22 concentration of WSBrC was considered as the concentration of WSOC.

23 After the extraction of WSBrC, the WI-MSBrC was extracted into 30 ml methanol using the
24 same filter sample left in the same glass bottle with screw cap sealed with Teflon tape under
25 ultrasonication for 30 min. The extracts were filtered using the same 0.45 μm PTFE syringe filter
26 to remove the insoluble particles and filter debris and transferred into another clean glass bottle.
27 The methanol extracts were used for the measurements of optical properties of WI-MSBrC. The
28 concentration of water-insoluble organic carbon (WIOC) was considered as the concentration of
29 WI-MSBrC, which calculated as: WI-MSBrC = OC - WSOC, presuming that all the water-
30 insoluble organic contents are dissolved in methanol, although we do not preclude that some of
31 organic species are not soluble in MeOH (Shetty et al., 2019).

32 2.3.2 Light absorption of BrC

33 A three-dimensional fluorescence spectrometer (Aqualog, Horiba Scientific) was used to
34 record the excitation-emission matrices (EEM) spectra and ultraviolet-visible (UV-Vis)
35 absorption spectra of the solution samples in 1×1 cm quartz cuvettes. The instrument parameters
36 during sample analysis were as follows: The UV-Vis absorption spectra of extracts were recorded
37 in the wavelength range of 240–700 nm. The UV-visible absorption spectra of the solvents were
38 also recorded to subtract their contributions from the extract spectra. The EEM was recorded in
39 the wavelength range of 240–700 nm for excitation and the integration time was 0.1 s with a 1 nm
40 increment. An increment of 8 pixels (5.04 nm) is used as the emission wavelength interval. Prior

1 to sample analysis, the pure solvents of water and methanol (MeOH) were used to obtain the
2 reference signal.

3 Based on the light absorption spectra, the absorption data are converted to the absorption
4 coefficient (Abs: m^{-1}) following this formula (Deng et al., 2022; Hecobian et al., 2010):

$$5 \quad \text{Abs}_\lambda = (A_\lambda - A_{700}) \times V_1 / V_a / L \times \ln(10)$$

6 where A_{700} is the absorption at 700 nm, serving as a reference to account for baseline drift;
7 V_1 is the volume of water or MeOH used for extraction; V_a is the volume of sampled air; L is the
8 optical path length (0.01 m). A factor of $\ln(10)$ is utilized to convert the log base 10 to a natural
9 logarithm to obtain a base-e absorption coefficient. To compensate for any baseline shift that may
10 occur during analysis, absorption at wavelengths below 700 nm is compared to that of 700 nm
11 where no absorption occurs for ambient aerosol extracts. The average absorption coefficient
12 between 360 and 370 nm (Abs_{365}) is used to represent BrC absorption in order to avoid any
13 interferences from non-organic compounds (e.g., nitrate) and to be consistent with the literature
14 values (Huang et al., 2018).

15 Absorption Ångström exponent (AAE, Å) represents the spectral dependence of aerosol light
16 absorption. The spectral dependence of light absorption by chromophores in solution can be
17 described by the following equation:

$$18 \quad \text{Abs}_\lambda = C \times \lambda^{-\text{AAE}}$$

19 where C is a composition-dependent constant; λ is the wavelength (nm). The AAE of the filter
20 extracts is calculated by a formula in the wavelength range of 300–500 nm. The selected range
21 serves two purposes: (1) to prevent any interferences from non-organic compounds at lower
22 wavelengths; (2) to ensure a sufficient signal-noise ratio for the investigating samples (Huang
23 et al., 2018).

24 The mass absorption efficiency (MAE: $\text{m}^2 \text{g}^{-1}$) of the filter extract at wavelength of λ can be
25 characterized as:

$$26 \quad \text{MAE}_\lambda = \text{Abs}_\lambda / M$$

27 where M ($\mu\text{g m}^{-3}$) is the concentration of WSOC for water extracts and that of WIOC for
28 methanol extracts.

29 The imaginary part (k) of the refractive index ($m = n+ik$) is derived with the following
30 equation (Liu et al., 2013; Deng et al., 2022):

$$31 \quad k_\lambda = (\text{MAC} \times \rho \times \lambda) / 4\pi$$

32 where MAC is the mass-absorption cross section of WSBrC or WI-MSBrC ($\text{m}^2 \text{g}^{-1}$), ρ is the
33 effective density, λ is the wavelength for the computed MAC including WSBrC and WI-MSBrC.
34 For this study, an effective density of 1.5 g m^{-3} is assumed for WSBrC and WI-MSBrC in the
35 derivation (Liu et al., 2013). MAC values are computed for 365 nm.

36 2.3.2 EEM of BrC and PARAFAC analysis

37 The raw EEMs were first calibrated for the correction of spectrometer factors, which reflect
38 the spectrometer deviation and light source, and then for the inner filter correction, following the
39 procedure described elsewhere (Chen et al., 2019; Gu and Kenny, 2009). Briefly, the inner filter
40 correction of the EEMs was done based on the UV-Vis light absorbance of the extracts, which was
41 lower than 0.7 in the calibrated wavelength range and is appropriate (Gu and Kenny, 2009). The
42 signal intensity of the EEMs was then normalized to the Raman unit (RU) of water (Lawaetz and
43 Stedmon, 2009). The fluorescence volume (FV, $\text{RU-nm}^2/\text{m}^3$) of extracts present in the atmosphere
44 was estimated based on the EEMs at the excitation wavelength ranging from 240 to 700 nm, and

1 then normalized it (i.e., NFV (RU-nm²-[mg/L]⁻¹)) by dividing the FV with the concentration of
2 WSOC and WIOC in the aerosol [mg m⁻³]).

3 Various types of chromophores present in the PM_{2.5} samples were classified and identified
4 based on the PARAFAC analysis of the EEMs using the SOLO (Eigenvector Inc.), the data
5 analysis software. PARAFAC analysis was performed for each extraction fluid in each season.
6 Ultimately, three EEM components were determined and assigned to different types of
7 chromophores.

8 Additionally, fluorescence index (FI) was determined by calculating the ratio of emission
9 intensities at 450 nm and 500 nm after excitation at 370 nm. Contributions from local biological
10 sources can be characterized by biological index (BIX), which was calculated using the ratio of
11 emission intensities at 380 and 430 nm following 310 nm excitation (Gao Yan and Zhang, 2018).
12 Under the condition of Ex=255 nm, the humification index (HIX) was determined by dividing the
13 area of fluorescence intensity between 435 and 480 nm by that of fluorescence intensity between
14 300 and 345 nm.

15 2.3.3 Simple forcing efficiency (SFE)

16 It is possible to make a rough estimate of the radiative forcing caused by aerosols using a
17 simple forcing efficiency (SFE, W/g), which reflects the energy added to the Earth's atmospheric
18 system per unit mass of aerosols and can be estimated as described in the literature (Bond and
19 Bergstrom, 2006; Deng et al., 2022), using the following equation:

$$20 \frac{dSFE}{d\lambda} = -\frac{1}{4} \frac{dS(\lambda)}{d\lambda} \tau_{atm}^2 (\lambda)(1 - F_c) \left[2(1 - a_s)^2 \beta(\lambda) \square MSC(\lambda) - 4a_s \square MAC(\lambda) \right]$$

21 where dS/dλ is the solar irradiance, τ_{atm} is the atmospheric transmission (0.79), F_c is the cloud
22 fraction (approximately 0.6), a is the surface albedo (average 0.19), β is the backscatter fraction,
23 and MSE and MAE are the mass scattering and absorption efficiency, respectively.

24 Since BrC causes the radiative effect by light absorption only, the direct radiative forcing due
25 to aerosol scattering can be ignored when estimating the radiative effect of the BrC. Therefore, the
26 equation can be simplified to:

$$27 SFE = \int \frac{dS(\lambda)}{d\lambda} \tau_{atm}^2 (1 - F_c) a_s MAE(\lambda) d\lambda$$

29 3 Results and discussion

30 3.1 Characteristics of ultraviolet light absorption of WSBrc and WI-MSBrC

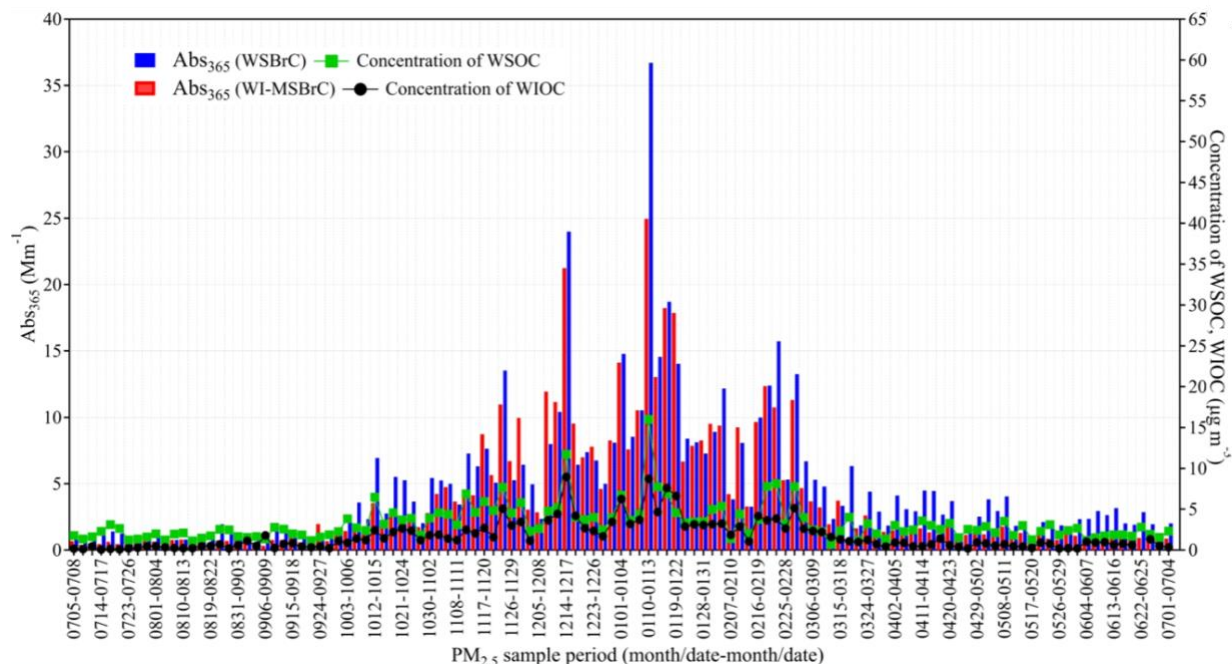
31 3.1.1 Absorption coefficient (Abs)

32 Annual and seasonal averages of various optical properties of WSBrc and WI-MSBrC in
33 PM_{2.5} measured in this study are summarized in Table 1. Their ranges and median values are
34 provided in supplement Table S1. Temporal variations in absorption coefficient of WSBrc at 365
35 nm (Abs₃₆₅(WSBrC)) and that of WI-MSBrC (Abs₃₆₅(WI-MSBrC)) together with the concentrations of
36 WSOC and WIOC are depicted in Fig. 1. Because the light absorption at the wavelength of 365
37 nm would not be interfered by inorganic substances (Hecobian et al., 2010), the Abs at 365 nm
38 was selected for the analysis in this study. Abs₃₆₅(WSBrC) ranged from 0.49 Mm⁻¹ to 36.7 Mm⁻¹ with

1 an average of 4.74 Mm^{-1} during the campaign. While the $\text{Abs}_{365(\text{WI-MSBrC})}$ ranged from 0.32–25.0
2 Mm^{-1} (ave. 3.87 Mm^{-1}) during the campaign. Temporal trends of $\text{Abs}_{365(\text{WSBrC})}$ were found to be
3 similar with those of $\text{Abs}_{365(\text{WI-MSBrC})}$, with the lowest levels in summer followed by a gradual
4 increase toward autumn and peak in winter and then a gradual decrease toward spring during the
5 campaign (Fig. 1). Furthermore, those trends were highly comparable to those of the
6 concentrations of both WSOC and WIOC in $\text{PM}_{2.5}$ (Fig. 1). The correlations between $\text{Abs}_{365(\text{WSBrC})}$
7 and WSOC and $\text{Abs}_{365(\text{WI-MSBrC})}$ and WIOC were found to be strong ($R = 0.93$ and 0.96 ,
8 respectively) during the campaign. These results indicate that both WSBrC and WI-MSBrC might
9 have been derived from the same or similar sources including the secondary processes, and their
10 light absorbance should have been significantly dependent on their abundances that varied from
11 season to season (Fig. 1; Table 1).

12 Averages of both $\text{Abs}_{365(\text{WSBrC})}$ and $\text{Abs}_{365(\text{WI-MSBrC})}$ were higher in winter followed by autumn
13 and spring and the lowest in summer (Table 1). The high Abs_{365} of BrC in winter might have been
14 mainly driven by the existence of large amounts of organic aerosols, whereas the lowest Abs_{365} in
15 summer might be due to enhanced decomposition of BrC constituents by photobleaching under
16 high solar radiation and oxidants loading in the atmosphere, which is unlikely in the wintertime.
17 The seasonal variations of both $\text{Abs}_{365(\text{WSBrC})}$ and $\text{Abs}_{365(\text{WI-MSBrC})}$ in Tianjin were similar to those
18 of the Abs_{365} of WSBrC reported in the southeastern United States, but their values (Table 1) were
19 much higher than that ($0.3\text{--}3.0 \text{ Mm}^{-1}$ in 2007) in the southeastern United States (Hecobian et al.,
20 2010) as well as that in Atlanta and Los Angeles (0.88 ± 0.71 and $0.61 \pm 0.38 \text{ Mm}^{-1}$, respectively)
21 in summer 2010 (Zhang et al., 2011). Biomass burning was considered to be the dominant source
22 of BrC at the southeastern United States in colder period, whereas both primary emissions from
23 fossil fuel combustion and secondary formation were significant in summertime (Hecobian et al.,
24 2010). While the SOA formed from fresh anthropogenic and biogenic VOCs were considered to
25 be major at Atlanta and Los Angeles, respectively (Zhang et al., 2011).

26 It has been reported that the solid fuels (i.e., biomass or coal) combustion is dominant and the
27 Abs_{370} of BrC is reported to be high (21.8 Mm^{-1}) in North China cities (Zhang et al., 2021). It has
28 also been reported that the Abs_{370} of BrC produced by residential wood burning is much higher,
29 reaching up to $37.1 \pm 74.6 \text{ Mm}^{-1}$ in Athens in winter (Liakakou et al., 2020). The maximum
30 $\text{Abs}_{365(\text{WSBrC})}$ and $\text{Abs}_{365(\text{WI-MSBrC})}$ in Tianjin aerosols were 36.7 and 25.0, respectively, which are
31 comparable to those of wood combustion samples. However, their ranges found to be large during
32 the campaign (Fig. 1; Table S1), suggesting that in addition to biomass burning, the other emission
33 sources and meteorological conditions in different seasons should have been played an important
34 role in controlling the WSBrC and WI-MSBrC loadings and their optical characteristics in the
35 Tianjin atmosphere. Furthermore, the $\text{Abs}_{365(\text{WSBrC})}$ observed in this study (Table 1) is slightly
36 lower compared to that reported in Tianjin during winter 2016 ($14.1 \pm 8.5 \text{ Mm}^{-1}$) and summer
37 2017 ($2.1 \pm 1.0 \text{ Mm}^{-1}$) (Deng et al., 2022) as well as that reported in Beijing and Xi'an, which are
38 considered to be highly polluted cities in northern China (Huang et al., 2020; Li et al., 2020b).
39 However, the $\text{Abs}_{365(\text{WSBrC})}$ and $\text{Abs}_{365(\text{WI-MSBrC})}$ found in winter in this study were higher than that
40 reported at different locations in southern China; Nanjing ($\text{Abs}_{365(\text{WSBrC})} = 4.84 \text{ Mm}^{-1}$,
41 $\text{Abs}_{365(\text{MSBrC})} = 7.75 \text{ Mm}^{-1}$) (Xie et al., 2020), Guangzhou ($\text{Abs}_{365(\text{WSBrC})} = 8.8 \text{ Mm}^{-1}$) (Li et al.,
42 2018), and Lhasa ($\text{Abs}_{365(\text{WSBrC})} = 1.04 \text{ Mm}^{-1}$, $\text{Abs}_{365(\text{MSBrC})} = 1.47 \text{ Mm}^{-1}$) (Zhu et al., 2018), where
43 the fossil fuel combustion is considered as the dominant source. Such higher Abs_{365} , particularly
44 in winter, indicates that BrC in $\text{PM}_{2.5}$ in Tianjin might have been derived from mixed sources such
45 as biomass burning and fossil fuel (coal) combustion and has a significant effect on light absorption
46 and thus on climate system over the region.

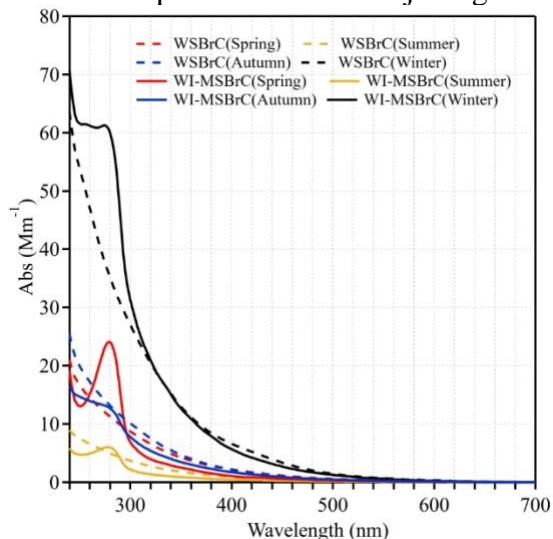


1
 2 **Figure 1.** Temporal variations of the light absorption coefficient of water-soluble brown carbon
 3 (BrC) at 365 nm ($Abs_{365}(WSBrC)$) and water-insoluble but methanol-soluble BrC ($Abs_{365}(WI-MSBrC)$)
 4 and the mass concentrations of WSOC and WIOC in $PM_{2.5}$ in Tianjin, North China during 2018
 5 and 2019. WSOC and WIOC mass concentrations data was obtained from (Dong et al., 2023b).

6 Figure 2 shows the seasonal average absorption spectra of WSBrC and WI-MSBrC at
 7 wavelengths of 240–700 nm, which shows a common feature that the absorption of shorter
 8 wavelengths increases sharply and significantly. Such feature is different from the absorption
 9 characteristics of BC, whose AAE is close to 1 and weakly dependent on the wavelength. Another
 10 evident feature of BrC absorption spectra shown in Figure 2 is that the Abs of WI-MSBrC was
 11 always greater than that of WSBrC across the shorter wavelengths in winter and in the range of
 12 260~300 nm in other seasons, which is consistent with the pattern reported in the literature (Huang
 13 et al., 2020; Li et al., 2020b). In addition, the Abs of WI-MSBrC peaked at 280 nm, but not that of
 14 WSBrC (Fig. 2). Such patterns can be attributed to the difference in types and amounts of
 15 chromophores soluble in water and methanol (e.g., PAHs are soluble in methanol, but not in water).
 16 It is noteworthy that, $\pi-\pi^*$ electron transitions in the double bonds of aromatic compounds are the
 17 primary cause of light absorption in the wavelength range of 250–300 nm. It has been reported in
 18 another study that nitroaromatics have contributed 60% to the total absorbance in the 300-400 nm
 19 range (Hems et al., 2021). The electron transitions in phenolic arenes, aniline derivatives, polyenes
 20 and polycyclic aromatic hydrocarbons with two or more rings are responsible for the absorbance
 21 in the bands between 270 and 280 nm (Badel et al., 2009). Therefore, the differences observed in
 22 the Abs of WSBrC and WI-MSBrC imply that the aromatic and/or unsaturated aliphatic organic
 23 compounds are abundant in $PM_{2.5}$ in Tianjin, which are more soluble in MeOH than in water.

24 High correlations ($R = 0.73-0.97$) were found between Abs_{365} of both WSBrC and WI-
 25 MSBrC and WSOC and WIOC in each season, except in summer ($R = 0.20-0.62$) (Figure S1). As
 26 noted earlier, such linearity of Abs_{365} with WSOC and WIOC indicate that WSBrC and WI-
 27 MSBrC might have been derived from similar sources including the secondary processes over the

1 Tianjin region, except in summer, because the light absorption efficiency of organic compounds
2 of different origin are different and significantly depend on their secondary processes in the
3 atmosphere (Zhong and Jang, 2011). In fact, the Abs depends on the amount of BrC availability,
4 but not of total OC content. In summer, the BrC loading might be less due to either photobleaching
5 under the enhanced aging and/or less availability of N and/or S species to produce N- and S-
6 containing organics (BrC) in the atmosphere over the Tianjin region.



7
8 **Figure 2.** Seasonal averages of absorption spectra in the wavelength range of 240–700 nm of
9 WSBrC and WI-MSBrC in PM_{2.5} from Tianjin, North China.

10 The moderate to high positive correlations ($R = 0.51-0.92$) found between both $Abs_{365}(WSBrC)$
11 and $Abs_{365}(WI-MSBrC)$ and K^+ and Cl^- in all seasons, except between $Abs_{365}(WSBrC)$ and Cl^- in summer
12 ($R = 0.29$) (Fig. S2), suggest that biomass burning and coal combustion were major sources (Dong
13 et al., 2022) of BrC in the Tianjin region. The poor correlation between Abs_{365} and K^+ was driven
14 by two outliers obtained in K^+ data that might have occurred due to unknown biomass burning
15 events at local scale. In addition, the correlation between $Abs_{365}(WSBrC)$ and K^+ was relatively
16 stronger than that between the $Abs_{365}(WI-MSBrC)$ and K^+ , except in summer (Fig. S2), which support
17 that the chromophores, like nitrophenols, derived from biomass burning are potentially more
18 water-soluble (Li et al., 2020b). While the correlation between $Abs_{365}(WI-MSBrC)$ and Cl^- was
19 relatively stronger than that between $Abs_{365}(WSBrC)$ and Cl^- in spring and summer and comparable
20 in autumn, which suggest that the chromophores derived from fossil fuel (e.g., coal) combustion
21 are slightly more soluble in MeOH compared to that in water, and were abundant in the spring and
22 summer time in Tianjin.

23

Table 1. Mass concentrations of WSOC, WIOC and absorbance efficiency of WSBrC and WMSBrC (Ave. \pm SD) in PM_{2.5} from Tianjin, North China.

	Annual	Summer	Autumn	Winter	Spring
Concentrations					
WSOC ($\mu\text{g m}^{-3}$)	3.25 \pm 2.18	1.88 \pm 0.53	3.45 \pm 1.71	5.06 \pm 2.99	2.48 \pm 0.82
WIOC ($\mu\text{g m}^{-3}$)	1.68 \pm 1.77	0.43 \pm 0.32	1.55 \pm 1.04	3.74 \pm 2.09	0.88 \pm 0.63
Optical parameters					
Abs ₃₆₅ (Mm ⁻¹)	4.74 \pm 5.10	1.47 \pm 0.77	3.71 \pm 2.83	10.4 \pm 6.76	3.45 \pm 2.29
MAE ₃₆₅ (m ² g ⁻¹)	1.28 \pm 0.66	0.80 \pm 0.44	0.96 \pm 0.33	2.04 \pm 0.46	1.31 \pm 0.55
AAE (300–500 nm)	5.66 \pm 0.82	5.17 \pm 0.83	6.21 \pm 0.65	5.88 \pm 0.58	5.42 \pm 0.74
E ₂ /E ₃	5.36 \pm 0.91	5.64 \pm 1.21	5.78 \pm 0.83	5.19 \pm 0.44	4.83 \pm 0.64
FI	1.38 \pm 0.09	1.31 \pm 0.07	1.47 \pm 0.07	1.37 \pm 0.02	1.37 \pm 0.09
BIX	1.05 \pm 0.13	0.91 \pm 0.06	1.06 \pm 0.08	1.20 \pm 0.08	1.01 \pm 0.11
HIX	2.87 \pm 0.53	3.12 \pm 0.44	3.11 \pm 0.51	2.47 \pm 0.43	2.76 \pm 0.47
k ₃₆₅	0.056 \pm 0.029	0.035 \pm 0.020	0.042 \pm 0.015	0.089 \pm 0.021	0.057 \pm 0.024
SFE _{300–400} (W g ⁻¹)	1.95 \pm 1.02	1.21 \pm 0.67	1.99 \pm 0.84	3.12 \pm 0.71	1.46 \pm 0.52
SFE _{300–700} (W g ⁻¹)	4.97 \pm 2.71	3.68 \pm 2.58	5.12 \pm 2.17	7.60 \pm 2.17	3.39 \pm 1.42
WI-MSBrC					
Abs ₃₆₅ (Mm ⁻¹)	3.87 \pm 4.69	0.74 \pm 0.25	2.83 \pm 2.51	10.0 \pm 5.13	1.99 \pm 1.95
MAE ₃₆₅ (m ² g ⁻¹)	2.36 \pm 1.26	2.50 \pm 1.78	1.86 \pm 1.02	2.69 \pm 0.36	2.41 \pm 1.28
AAE (300–500 nm)	6.06 \pm 1.23	5.49 \pm 1.26	6.11 \pm 1.86	6.30 \pm 0.27	6.27 \pm 0.90
E ₂ /E ₃	6.60 \pm 2.04	6.79 \pm 1.32	5.77 \pm 1.35	6.20 \pm 0.44	7.60 \pm 3.25
FI	1.60 \pm 0.13	1.58 \pm 0.12	1.57 \pm 0.06	1.73 \pm 0.11	1.51 \pm 0.11
BIX	1.26 \pm 0.21	1.32 \pm 0.18	1.05 \pm 0.14	1.43 \pm 0.09	1.23 \pm 0.18
HIX	0.81 \pm 0.60	0.25 \pm 0.08	1.23 \pm 0.61	1.33 \pm 0.30	0.42 \pm 0.28
k ₃₆₅	0.104 \pm 0.057	0.109 \pm 0.079	0.081 \pm 0.045	0.117 \pm 0.016	0.105 \pm 0.057
SFE _{300–400} (W g ⁻¹)	2.98 \pm 1.70	1.21 \pm 0.67	2.98 \pm 1.52	4.13 \pm 0.57	3.61 \pm 1.91
SFE _{300–700} (W g ⁻¹)	7.58 \pm 5.75	3.68 \pm 2.58	8.69 \pm 9.23	9.36 \pm 4.51	8.70 \pm 5.03

3.1.2 Absorption Ångström exponent (AAE)

The magnitude of the AAE can reflect the sources and atmospheric chemical processes of BrC (Lack et al., 2013), because the AAE of the BrC emitted from fossil fuel combustion found to be ~ 1 and that from biomass burning range from 1 to 3 and that derived by secondary formation/transformations vary from 3-7 (Yan et al., 2018). It has also been reported that the AAE of light-absorbing organic species (i.e., BrC) is much larger than that of soot (BC). The AAE was found to be between 2 and 4 for the particles containing both soot and BrC. Furthermore, AAE value of particulate matter is closely related to its chemical composition, mixing state, particle size and other factors. *For example*, Sun et al. (2007) reported that the average AAE of coal briquettes is 2.55 ± 0.44 whereas that of the coal chunks is 1.30 ± 0.32 (Sun et al., 2017). However, it is important to note that unlike the direct measurement of AAE of the particulate matter, the light absorption characteristics of organic components extracted into solvent are not affected by particle size and mixing state of aerosols, but depend on their composition. The AAE of humic-like substances (HULIS) isolated from biomass burning aerosols by water extraction followed by the separation with exchange column was reported to be 6-7 (Hoffer et al., 2006).

The AAE of WSBrc in PM_{2.5} from Tianjin ranged from 3.85 to 7.99 with an average of 5.66 during the campaign. The seasonal averages were highly comparable with each other, except a little higher level in autumn (Table 1). The average AAE of WSBrc in Tianjin (Table 1) is comparable to that (5.1 ± 2.0) reported from New Delhi, India and Beijing (5.3 ± 0.4 in winter and 5.8 ± 0.5 in summer) and the outflow region (6.4 ± 0.6) of northern China (Lesworth et al., 2010). The AAE of WSBrc in Tianjin was also similar to that (range, 6–8) reported in the particulate matter at the southeastern United States (Hecobian et al., 2010) and downtown Atlanta (Liu et al., 2013), where both biogenic and fossil fuel combustion emissions and secondary processes are considered as significant sources. Such higher levels and comparisons of the AAE of WSBrc imply that the OA in Tianjin should have been derived from mixed sources and substantially polar, because the AAE of BrC is increased with its increasing polarity (Chen et al., 2016a).

However, the AAE of WI-MSBrC in Tianjin ranged from 2.08 12.9 (ave. 6.06) and was comparable with that of WSBrc. Furthermore, the averages of AAE of WI-MSBrC in each season were comparable with the other, except a relatively lower level in summer, and also with those of the AAE of WSBrc (Table 1). Such comparability between the AAE of WSBrc and WI-MSBrC is consistent with the pattern reported in urban Beijing during winter and Xi'an, China (Li et al., 2020b), where the emissions from fossil fuel combustion are dominant. These results and their comparisons again support that the BrC might have significantly derived from mixed sources (biomass burning and fossil fuel combustion). In fact, the AAE of the solvent (e.g., acetonitrile) extracted portion of the BrC derived from biomass burning is also large (Lin et al., 2017).

3.1.3 Mass absorption efficiency (MAE) and imaginary refractive index (k)

MAE provides the light absorbing ability of BrC. The MAE₃₆₅ of WSBrc (MAE_{365(WSBrc)}) ranged from $0.38 \text{ m}^2 \text{ g}^{-1}$ to 3.41 (ave. $1.28 \text{ m}^2 \text{ g}^{-1}$) and lower by 2 times than that (range, 0.18-7.05 $\text{m}^2 \text{ g}^{-1}$; ave. $2.36 \text{ m}^2 \text{ g}^{-1}$) of WI-MSBrC (MAE_{365(WI-MSBrC)}) during the campaign in Tianjin. Although the seasonal averages of both MAE_{365(WSBrc)} and MAE_{365(WI-MSBrC)} were higher in winter (1.28 and $2.36 \text{ m}^2 \text{ g}^{-1}$, respectively), the former showed the second most value in spring followed by autumn and the lowest value in summer, whereas the latter showed second most value in summer followed by spring and the lowest value in autumn (Table 1). Furthermore, the average MAE_{365(WSBrc)} in winter was 2.5 times higher than that in summer, which is similar to that (1.8

1 times) reported earlier in Tianjin (Deng et al., 2022), whereas the difference between the averages
2 of MAE_{365(WI-MSBrC)} in winter to autumn is 1.4 times only. The seasonal variations of MAE_{365(WSBrc)}
3 and MAE_{365(WI-MSBrC)} found in this study are similar to those reported in Xi'an (Li et al., 2020b).

4 The imaginary refractive index (k) is another important parameter that represent the light
5 absorbing ability of carbon and applied in climate model to assess the direct radiative forcing of
6 aerosols. The k of WSBrc ($k_{365(WSBrc)}$) and WI-MSBrC ($k_{365(WI-MSBrC)}$) in Tianjin ranged from
7 0.017 to 0.149 (ave. and 0.008-0.307, respectively, in Tianjin. Interestingly, the average $k_{365(WI-MSBrC)}$
8 was 1.9 times to that of $k_{365(WSBrc)}$ during the campaign (Table 1) and their seasonal patterns
9 were also exactly similar to those of the MAE_{365(WSBrc)} and MAE_{365(WI-MSBrC)} (Table 1).

10 Both these MAE₃₆₅ and k_{365} results indicate that most of light-absorbing chromophores are
11 insoluble in water but soluble in MeOH, and their abundances are significantly varied from season
12 to season. Such large seasonal differences indicate that the BrC sources and formation and/or
13 transformation including the degradation (photobleaching) processes might be different in each
14 season. The higher levels of MAE₃₆₅ and k_{365} in winter suggest that the contributions of OA from
15 coal combustion and biomass burning emissions were significantly higher than that in other
16 seasons due to increased residential heating activities. The lower MAE_{365(WSBrc)} and $k_{365(WSBrc)}$ and
17 the second most values of MAE_{365(WI-MSBrC)} and $k_{365(WI-MSBrC)}$ in summer imply that the
18 contributions of OA from fossil fuel combustion emissions might be dominant and the subsequent
19 photobleaching of WSBrc might be significant under high solar radiation in the summertime.

20 The ratio of MAE₂₅₀ to MAE₃₆₅, which is inversely correlate with the molecular size and
21 aromaticity (Chen et al., 2016c), of WSBrc ($E_2/E_{3(WSBrc)}$) and WI-MSBrC ($E_2/E_{3(WI-MSBrC)}$) in
22 Tianjin ranged from 3.30 to 6.25 with an average of 4.83 and 4.50-24.1 (ave. 7.61), respectively,
23 during the campaign. Interestingly, the averages of $E_2/E_{3(WSBrc)}$ were comparable in summer and
24 autumn and higher than that in winter and spring (Table 1). Whereas the average $E_2/E_{3(WI-MSBrC)}$
25 was higher in spring followed by summer and winter and the lowest in autumn, and higher than
26 the $E_2/E_{3(WSBrc)}$ in each season, except in autumn. Both $E_2/E_{3(WSBrc)}$ and $E_2/E_{3(WI-MSBrC)}$ in each
27 season were comparable or relatively higher than the E_2/E_3 of HULIS (4.7 ± 0.27 for herbaceous
28 plants, 3.6 ± 0.18 for shrubs, 4.2 ± 0.77 for evergreen trees, 4.0 ± 0.82 for deciduous trees, $5.8 \pm$
29 0.5 for rice straw, 4.5 ± 0.2 for corn straw and 4.4 ± 0.3 for pine branches) emitted from biomass
30 burning (Tang et al., 2020) and lower than that (14.7 ± 0.7) of HULIS emitted from coal
31 combustion (Fan et al., 2016). Thus, the $E_2/E_{3(WSBrc)}$ and $E_2/E_{3(WI-MSBrC)}$ and their comparisons
32 with source signatures indicate that both WSBrc and WI-MSBrC in PM_{2.5} over the Tianjin region
33 should have been mainly derived from biomass burning followed by coal combustion and consist
34 of high aromaticity and large in molecular size.

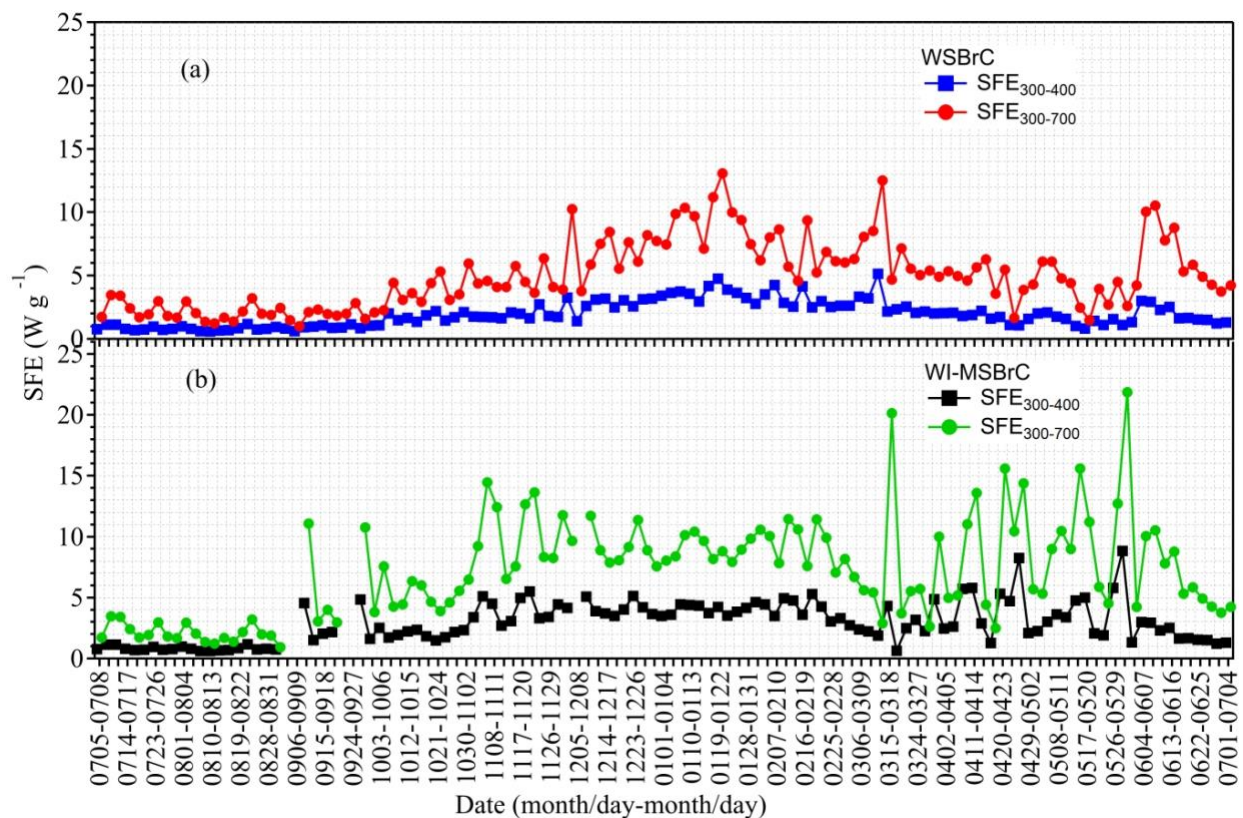
35 3.2 Direct radiative forcing of WSBrc and WI-MSBrC

36 Radiative forcing efficiency of WSBrc and WI-MSBrC were calculated by integrating the
37 wavelength dependent SFE from 300 nm to 700 nm ($SFE_{300-700(WSBrc)}$ and $SFE_{300-700(WI-MSBrC)}$,
38 respectively) in this study. The $SFE_{300-400}$ was also integrated to estimate the radiative forcing
39 efficiency of WSBrc ($SFE_{300-400(WSBrc)}$) and WI-MSBrC ($SFE_{300-400(WI-MSBrC)}$), because the BrC
40 strongly absorbs light in the UV-Vis range. The temporal variations of SFE of WSBrc and WI-
41 MSBrC in both the wavelength ranges are shown in Fig. 3. $SFE_{300-700(WSBrc)}$ and $SFE_{300-400(WSBrc)}$
42 ranged from 0.98 Wg^{-1} to 13.1 Wg^{-1} with an average of 4.97 Wg^{-1} and $0.60-5.13 \text{ Wg}^{-1}$ (ave. 1.95
43 Wg^{-1}), respectively. Whereas the $SFE_{300-700(WI-MSBrC)}$ and $SFE_{300-400(WI-MSBrC)}$ were $0.92-51.3 \text{ Wg}^{-1}$
44 (7.58 Wg^{-1}) and $0.64-8.84 \text{ Wg}^{-1}$ (2.98 Wg^{-1}), respectively, and were higher by 1.5 times than that
45 of the $SFE_{300-700(WSBrc)}$ and $SFE_{300-400(WSBrc)}$ (Table 1). Further both integrated average SFE_{300-

1 700(WSB_{rC}) and SFE₃₀₀₋₇₀₀(WI-MSB_{rC}) were higher by 2.5 times to that of the SFE₃₀₀₋₄₀₀(WSB_{rC}) and
2 SFE₃₀₀₋₄₀₀(WI-MSB_{rC}) (Table 1). Temporal variations of both the SFE₃₀₀₋₄₀₀(WSB_{rC}) and SFE₃₀₀₋₇₀₀(WSB_{rC})
3 700(WSB_{rC}) were found to be quite similar with a clear seasonal pattern with the lowest levels in
4 summer followed by a gradual increase toward autumn to peak in winter and then a gradual
5 decrease toward spring to the lowest levels in summer, except a sharp rise in early summer 2019
6 (Fig. 3). Whereas the SFE₃₀₀₋₄₀₀(WI-MSB_{rC}) and SFE₃₀₀₋₇₀₀(WI-MSB_{rC}) showed exactly the similar
7 temporal pattern with each other, but different from that of the SFE₃₀₀₋₄₀₀(WSB_{rC}) and SFE₃₀₀₋₇₀₀(WSB_{rC})
8 (Fig.3). The levels of SFE₃₀₀₋₄₀₀(WI-MSB_{rC}) and SFE₃₀₀₋₇₀₀(WI-MSB_{rC}) found to be relatively
9 stable throughout each season, except in spring, with higher level in spring followed by winter and
10 lower levels in summer (Fig. 3). In consistent with these seasonal patterns, the seasonal variations
11 of k_{365} (WSB_{rC}) and k_{365} (WI-MSB_{rC}), a vital parameter that reflect the light absorbing ability and used in
12 the estimation of radiative forcing by climatic model (Shamjad et al., 2016), were also showed the
13 similar pattern (Fig. S3).

14 The SFE of both WSB_{rC} and WI-MSB_{rC} in both the spectral ranges were higher in winter
15 (Table 1). However, SFE₃₀₀₋₄₀₀(WSB_{rC}) and SFE₃₀₀₋₇₀₀(WSB_{rC}) showed the second higher values in
16 autumn and the lowest and comparable values in summer and spring (Table 1). Whereas SFE₃₀₀₋₇₀₀(WSB_{rC})
17 400(WI-MSB_{rC}) and SFE₃₀₀₋₇₀₀(WI-MSB_{rC}) showed the second higher and comparable values in spring
18 and autumn and the lowest values in summer (Table 1). It is noteworthy that the SFE₃₀₀₋₄₀₀(WSB_{rC}),
19 SFE₃₀₀₋₇₀₀(WSB_{rC}), SFE₃₀₀₋₄₀₀(WI-MSB_{rC}) and SFE₃₀₀₋₇₀₀(WSB_{rC}) were higher by 61%, 52%, 71% and
20 61%, respectively, in winter than those in summer, indicating that BrC abundance and strong light
21 absorption capacity of BrC in winter led to a significant increase in direct radiative forcing by the
22 BrC. Furthermore, SFE₃₀₀₋₄₀₀ accounted for 40% of SFE₃₀₀₋₇₀₀ in both the fractions of BrC during
23 the whole campaign period and their seasonal averages varied between 33-44%, which are similar
24 to that reported in Tianjin by Deng et al. (2022), indicating the light absorption by BrC in UV-Vis
25 range play a significant role in the total BrC radiative forcing.

26 Furthermore, it is important to note that it has been reported that direct radiative effect of
27 WSB_{rC} is 12.5% and 13.5% relative to black carbon (BC) radiative forcing in the 280-4000 nm
28 range in summer and winter, respectively, in Tianjin (Deng et al., 2022). In fact, as noted above,
29 the annual average SFE₃₀₀₋₇₀₀(WI-MSB_{rC}) is higher by 1.5 times to that of SFE₃₀₀₋₇₀₀(WSB_{rC}) (Table 1)
30 in Tianjin. Therefore, the direct radiative effect of total (Σ WSB_{rC}+WI-MSB_{rC}) BrC relative to to
31 BC would become ~32.5% in Tianjin, revealing that the BrC play a greater role in light absorbing
32 aerosols in the shorter wavelength region in comparison to the entire spectrum.



1
 2 **Figure 3.** Temporal variations in SFE of WSBrc and WI-MSBrc from 300–400nm and 300–
 3 700nm in PM_{2.5} from Tianjin.

4 3.3 Fluorescence characteristics of WSBrc and WI-MSBrc

5 3.3.1 Fluorescence indices

6 Annual and seasonal averages of the fluorescence indices: FI, BIX and HIX, of WSBrc
 7 (FI_{WSBrc}, BIX_{WSBrc} and HIX_{WSBrc}, respectively) and WI-MSBrc (FI_{WI-MSBrc}, BIX_{WI-MSBrc} and
 8 HIX_{WI-MSBrc}, respectively) in PM_{2.5} at Tianjin are presented in Table 1. Their ranges and median
 9 values are provided in Table S1, and temporal variations are depicted in Fig. 3. Fluorescence
 10 indices are developed as indicators for the type and source of the fluorescent organic matter (OM)
 11 in aquatic and soil systems and has been successfully applied to assess the sources and aging
 12 processes of OA in the atmosphere in recent times (Dong et al., 2023b; Lee et al., 2013; Wu et al.,
 13 2021b). FI and BIX provide the insights in exploring the source and aging of OA and received
 14 much attention in recent times (Xie et al., 2020; Gao Yan and Zhang, 2018; Qin et al., 2018; Deng
 15 et al., 2022). They have been considered as indicators to assess the relative contributions of
 16 terrestrial, biological and microbially derived OM to OA. The FI values of OM lower than 1.4
 17 indicate its terrestrial origin and the values of 1.9 or higher indicate the microbial origin, and shows
 18 an inverse relationship with aromaticity of the OM (Gao Yan and Zhang, 2018; Birdwell and
 19 Engel, 2010). The BIX values of 0.8 and 1.0 correspond to the freshly derived OM of biological
 20 or microbial origin and those of ~0.6 imply the little contribution of the biological OM (Birdwell
 21 and Engel, 2010; Dong et al., 2023b). HIX reflect the degree of humification of OA, and has been
 22 considered as a proxy for aromaticity of OM and the HIX value is increased with the increasing

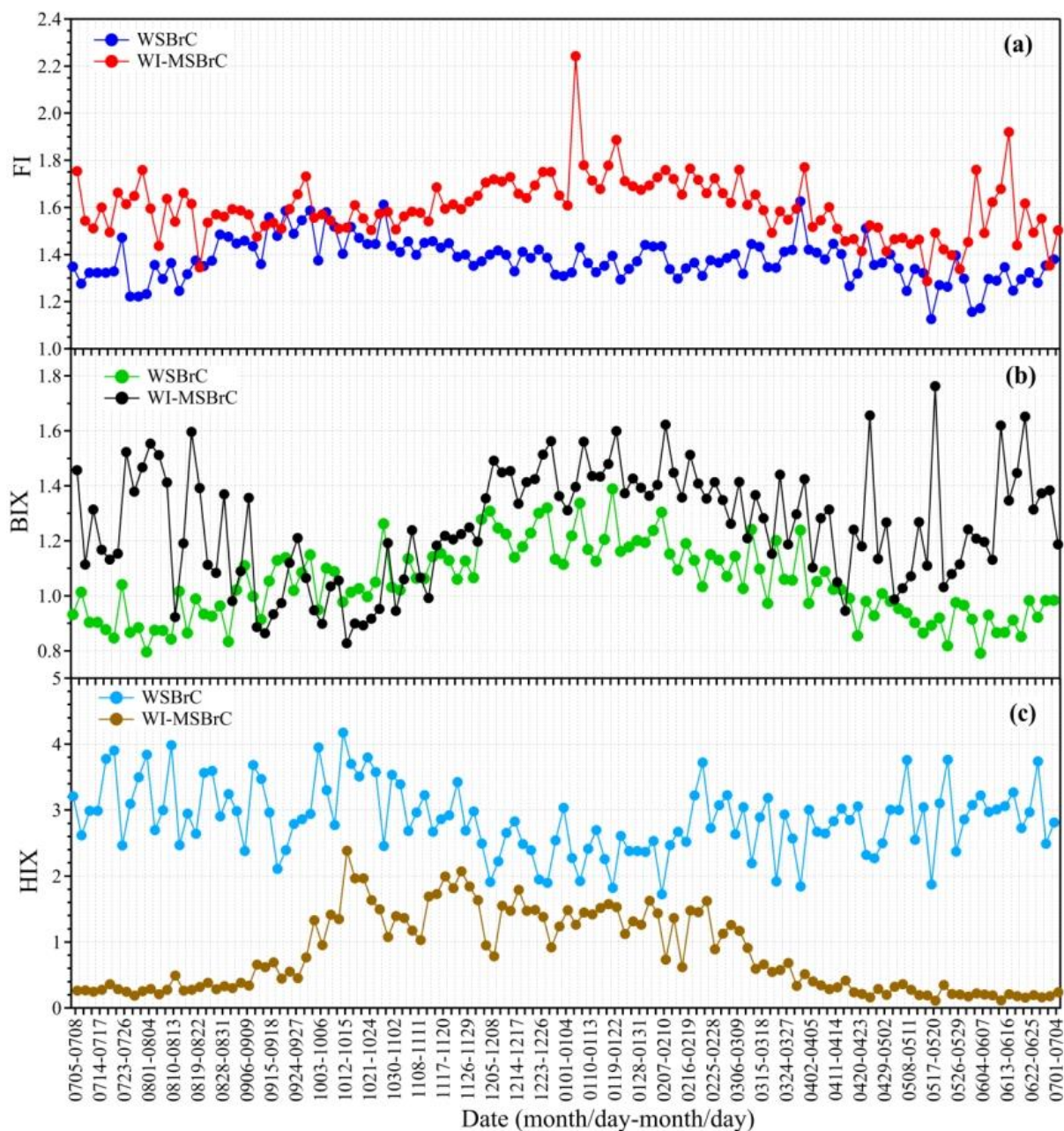
1 aromaticity and polycondensation degree (Deng et al., 2022; Mcknight et al., 2001; Birdwell and
2 Engel, 2010). The HIX values of >5 reflect the fresh OM derived from biomass and animal manure
3 (Birdwell and Engel, 2010).

4 FI_{WSBrC} and $FI_{WI-MSBrC}$ were ranged from 1.13 to 1.63 with an average of 1.38 and 1.29-2.24
5 (ave. 1.60), respectively, during the campaign in Tianjin. While BIX_{WSBrC} and $BIX_{WI-MSBrC}$ were
6 0.79-1.39 (1.05) and 0.83-1.76 (1.26), respectively, during the campaign. Both FI and BIX of
7 $WSBrC$ and $WI-MSBrC$ followed a temporal pattern, but the temporal pattern of FI_{WSBrC} was
8 exactly opposite to that of the $FI_{WI-MSBrC}$ (Fig. 4a). The FI_{WSBrC} values were slightly decreased
9 from summer to autumn followed by a gradual increase to mid-winter and then a gradual decrease
10 to summer through spring (Fig. 4a). While the temporal variations of BIX_{WSBrC} showed a gradual
11 decrease from summer to autumn followed by a gradual increase to winter and remained relatively
12 stable during the wintertime followed by a gradual decrease to to summer through spring (Fig. 4b).
13 The temporal variations of $BIX_{WI-MSBrC}$ were also found to be opposite to those of the BIX_{WSBrC} ,
14 except in winter, in which the $BIX_{WI-MSBrC}$ values were higher compared to those in other seasons
15 (Fig. 4b). Interestingly, the temporal patterns of HIX_{WSBrC} and $HIX_{WI-MSBrC}$ were found to be
16 similar with relatively stable in summer followed by a sharp increase in early autumn and then a
17 gradual decrease to summer through winter and spring (Fig. 4c). Further the HIX_{WSBrC} was always
18 significantly higher than the $HIX_{WI-MSBrC}$. Such temporal differences in all the three fluorescence
19 indices clearly indicate that the composition and/or aromaticity of $WSBrC$ and $WI-MSBrC$ are
20 substantially distinct, even though they might have been mainly derived from similar sources:
21 biomass burning and coal combustion, as discussed in previous section.

22 Average FI_{WSBrC} was found to be higher in autumn followed the similar levels in winter and
23 spring and the lowest in summer, whereas that of BIX_{WSBrC} was higher in winter followed by
24 autumn, spring and the lowest in summer (Table 1). While the averages of both $FI_{WI-MSBrC}$ and
25 $BIX_{WI-MSBrC}$ were higher in winter followed by summer, spring and the lowest in autumn (Table
26 1). Annual and seasonal averages of FI values of both $WSBrC$ and $WI-MSBrC$ were around or
27 higher than 1.4 and lower than 1.9 in Tianjin, indicating that the BrC in Tianjin was mainly derived
28 from terrestrial OM that should have largely consist of high aromatic compounds. In contrast, the
29 annual and seasonal averages of BIX of both $WSBrC$ and $WI-MSBrC$ were higher than 1.0 (Table
30 1), indicating the predominant contributions of OM from the biological (including biomass
31 burning) sources. In addition, the lowest FI_{WSBrC} and BIX_{WSBrC} values in summer and those of the
32 $FI_{WI-MSBrC}$ in spring and $BIX_{WI-MSBrC}$ in autumn suggest that the contribution from terrestrial
33 sources (e.g., coal combustion) might be less in spring and autumn and the photobleaching of OA
34 might be significant under high solar radiation in summer.

35 HIX_{WSBrC} and $HIX_{WI-MSBrC}$ were ranged from 1.72 to 4.7 with an average of 2.87 and
36 0.11-2.38 (ave. 0.81), respectively, during the campaign, which again support that both the BrC
37 components in Tianjin should have been significantly derived from biomass burning and might
38 consist highly humified and aromatic compounds. Average HIX_{WSBrC} was higher in summer
39 followed by autumn, spring and the lowest in winter (Table 1). In contrast, the average $HIX_{WI-MSBrC}$
40 was higher in winter followed by autumn, spring and the lowest in summer (Table 1). It has
41 been reported that aging processes and HIX have a significant relation (Deng et al., 2022). The
42 higher HIX_{WSBrC} and lower $HIX_{WI-MSBrC}$ in summer confirm that the BrC, which is more water-
43 soluble, was significantly produced from aromatic compounds and subjected for significant
44 atmospheric aging in summer over the Tianjin region.

45

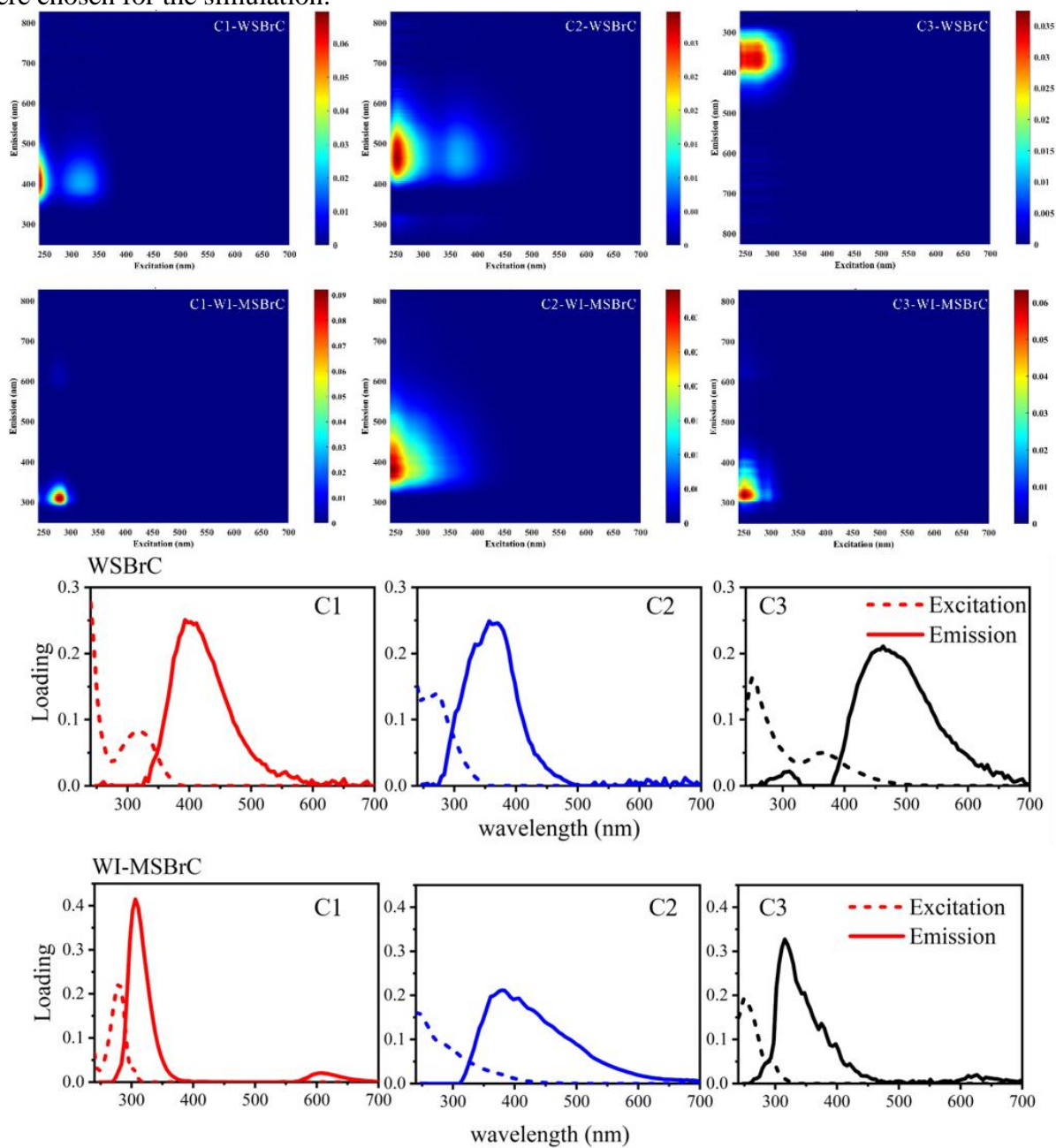


1
 2 **Figure 4.** Temporal variations in light absorption and fluorescence properties of BrC in PM_{2.5}
 3 Tianjin: (a) FI, (b) BIX, and (c) HIX.

4 3.3.2 Fluorophore identification

5 It is well established that fluorophores with different excitation emission wavelengths can
 6 distinguish their types and sources. However, the types and sources of a large number of
 7 fluorophores have not been determined due to their complex chemical composition and sources.
 8 Here, we separated several fluorescence components from the EEM data using the parallel factor
 9 analysis (PARAFAC) model, and the results are shown in Fig. 5. The fact of the value of core
 10 consistency close to 100 in PARAFAC model indicates that the more the individual components

1 that are analyzed together make up 100% of the mixture, with no unexplained residues. The core
 2 consistency of PARAFAC model explained the maximum variance of 89% for WSBrc and of
 3 95% for WI-MSBrC whole data obtained during the campaign, when three independent groups
 4 were chosen for the simulation.



5
 6 **Figure 5.** Three-dimensional excitation-emission matrix of three fluorescent components with
 7 emission in WSBrc (above) and WI-MSBrC (below) obtained by PARAFAC model analysis.

8 The types of fluorophores of both WSBrc and WI-MSBrC identified in this study together
 9 with their excitation and emission wavelengths and those reported in the literature are summarized
 10 in Table 2. Among the total of three types of fluorophores obtained for WSBrc in Tianjin PM_{2.5}

1 by PARAFAC for EEMs, two showed the fluorescence characteristics similar to those of less
 2 oxygenated and highly oxygenated humic-like substances (HULIS), respectively, and the third one
 3 showed similar to those of protein compounds (PLOM). Fluorophore C1_{WSBrC} has a primary
 4 fluorescence peak at excitation/emission (Ex/Em): <240/393 nm, and a secondary fluorescence
 5 peak at Ex/Em: 318/393 nm. C1_{WSBrC} can be classified as a humus-like fluorophore because the
 6 bimodal distribution of the fluorescence spectrum is usually associated with HULIS. The emission
 7 wavelength of C1_{WSBrC} was closer to the UV region than that of the second peak of C2_{WSBrC},
 8 indicating the existence of a small number of aromatic substances, conjugate systems and
 9 nonlinear ring systems (Deng et al., 2022). C2_{WSBrC} (Ex/Em ~251, 363 nm/462 nm) was identified
 10 as a common HULIS in aerosols, with higher oxidation, aromatization, molecular weight,
 11 conjugation, and unsaturation due to its larger emission wavelength (Wen et al., 2021). The
 12 molecular weight of the fluorophore as well as its degree of conjugation tend to increase with the
 13 excitation wavelength, and such increase in size and the conjugation degree may be attributed to
 14 the presence of highly aromatic conjugated structures containing heteroatoms (Chen et al., 2019).
 15 Compared to C1_{WSBrC} and C2_{WSBrC}, C3_{WSBrC} also contains two peaks, with shorter wavelengths
 16 (<380 nm) emission peak, which is usually associated with protein-like organic matter (PLOM)
 17 such as tryptophan and tyrosine, with low aromatic properties and small molecular size (Table 2).
 18

19 **Table 2.** Description and wavelength positions of PARAFAC components in this study and other
 20 reports from the literature. (PLOM = protein compounds; HULIS = humic-like substances)

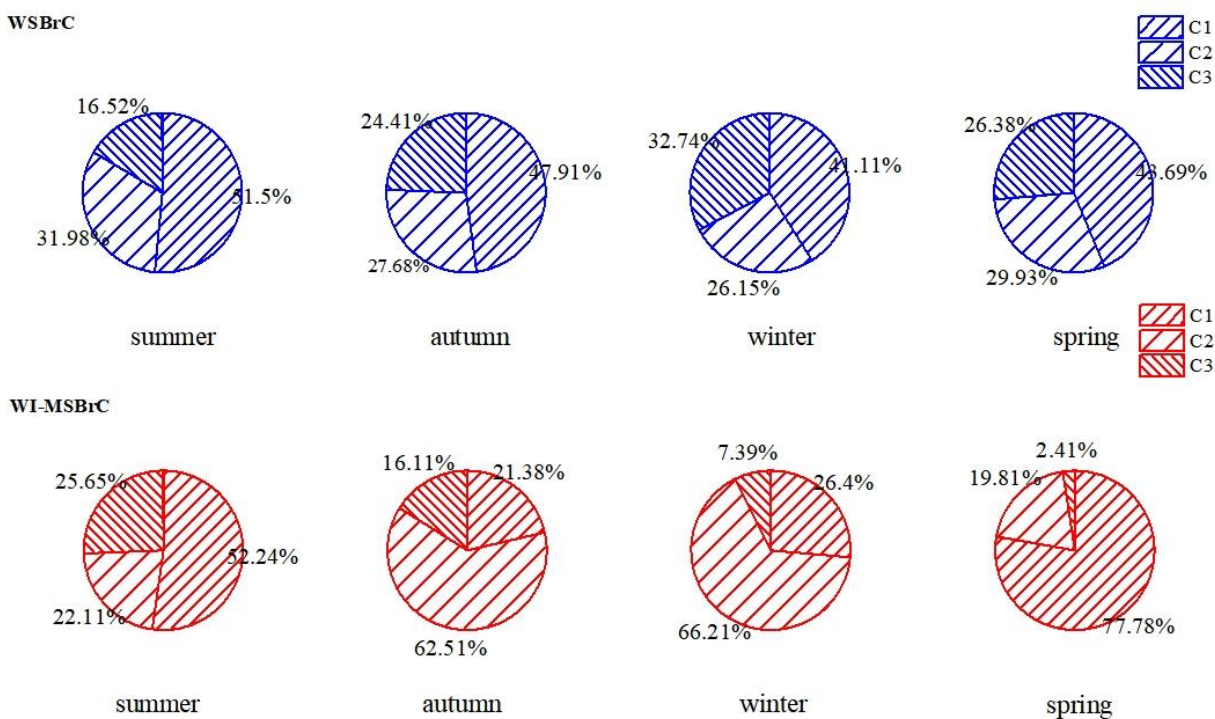
Category	Components	Ex(nm)	Em(nm)	Substances	References
WSBrC	C1	<240, 318	393	low-oxygenated HULIS	this study
	C2	251, 363	462	high-oxygenated HULIS	
	C3	<240, 271	356.3	PLOM, such as tryptophan and tyrosine	
WI-MSBrC	C1	<240, 279	306	PLOM, tyrosine-like	this study
	C2	<240	379	uncertain	
	C3	251, 294	315	PLOM, tryptophan-like	
Water-soluble BrC	C1	250, 315	396	low-oxygenated HULIS	(Deng et al., 2022)
	C2	250	465	highly-oxygenated HULIS	
	C3	250	385	low-oxygenated HULIS	
	C4	250	340	PLOM, tryptophan-like	
	C5	275	305	PLOM, tyrosine-like	
WSOC	C1	240, 315	393	low-oxygenated HULIS	(Wen et al., 2021)
	C2	245, 360	476	highly-oxygenated HULIS	
	C3	<240, 290	361	PLOM, such as tryptophan and tyrosine	
	C4	275	311	PLOM, tyrosine-like	
WSM and MSM	C1	255	415	HULIS-1 component	(Chen et al., 2019)
	C2	220	340	tryptophan-like component	
	C3	255	385	HULIS-2 component	
	C4	210	300	tyrosine-like component	
	C5	250	355	amino acid-like component	
WSOC	C1	245	410	HULIS, photodegradation of macromolecules	(Xie et al., 2020)
	C2	235	398	HULIS, aromatic and saturated compounds were presented	
	C3	250, 360	466	humic-like chromophores, more aromatic and consisted of more unsaturated compounds produced by condensation reactions	
	C4	250, 285	432	terrestrial humic-like chromophore	
	C5	<235	430	terrestrial humic-like substance, photochemical product	
MSOC	C6	275	408	low oxidation humic-like	
	C7	235, 275	372	protein-like chromophore	
	C8	260, 310	364	protein-like (tryptophan-like), may be related to PAHs	

21
 22 However, WI-MSBrC fluorophore C1_{WI-MSBrC} might be tyrosine-like substance. C2_{WI-MSBrC}
 23 is not quite certain and could be either HULIS or PLOM, because its emission wavelength <380

1 nm generally fits the profile of PLOM, but it is also close to the emission wavelength of HULIS
 2 (Table 2). While C3_{WI-MSBrC} is a tryptophan-like substance, which was reported to contain less
 3 aromatic and small molecular weight compounds. In general, phenols contribute significantly to
 4 C3_{WI-MSBrC} fluorophore as they are the products of incomplete pyrolysis of lignin and cellulose and
 5 are used as indicators of biomass burning (Wen et al., 2021). Therefore, WI-MSBrC fluorophores
 6 of all samples in this study can be classified as mainly PLOM.

7 The percent contributions of each fluorophore to WSBrc and WI-MSBrC in PM_{2.5} in Tianjin
 8 in each season are shown in Fig. 6. The compositions of WSBrc and WI-BrC clearly imply that
 9 the former contained more HULIS, whereas the later consist mostly of PLOM, and also indicate
 10 that most of the fluorophores of protein-like substances could dissolve in organic solvent, rather
 11 than in water.

12 According to the excitation emission wavelength, we classified the fluorescence component
 13 of WI-MSBrC substance as PLOM, but the correlation between their fluorescence intensity and
 14 BIX ($R = 0.66, p < 0.05$) was very small, far lower than that of WSBrc substance and BIX ($R =$
 15 $0.59, p < 0.05$). On the contrary, the correlation between their fluorescence intensity and HIX ($R =$
 16 $0.74, p < 0.05$) was much higher than that of WSBrc ($R = -0.10, p < 0.05$). Although PLOM
 17 may be associated with some polycyclic aromatic hydrocarbons (PAHs) or phenols from fossil
 18 fuel combustion and biomass burning, especially in urban aerosols, the correlation is puzzling.



21 **Figure 6.** Relative abundances of the chromophores of the WSBrc and WI-MSBrC in PM_{2.5}
 22 from Tianjin.

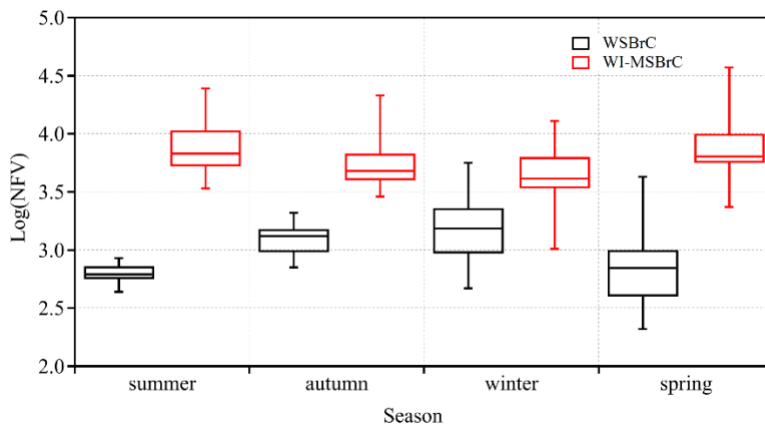
23 On average, the humic-like fluorophores together contributed more than 60% to the
 24 fluorescence intensity in WSBrc, suggesting that humic-like fluorophores played a dominant role
 25 in fluorescence properties of WSBrc in Tianjin. Generally, the low-oxygenated fluorophores
 26 C1_{WSBrC} made considerable contributions in each season. While C2_{WSBrC}, highly oxygenated

1 HULIS, has a greater relative contribution in summer, which might be due to the strong solar
2 radiation in summer. In contrast, in WI-MSBrC, the average contribution of PLOM to fluorescence
3 intensity was higher than 70% in spring (80.2%) and summer (77.9%), but C2_{WI-MSBrC} component
4 dominated in winter and autumn. This indicated that biological activities increased in spring and
5 summer and the relative abundance of bioaerosols might be higher during that period.

6 3.4 Potential sources of BrC

7 To further explore the potential sources of BrC, correlations of FV with chemical components
8 and light absorption of PM_{2.5} were examined. The sum of FVs of WSBrc and WI-MSBrC
9 (FV_{S(WSBrc+WI-MSBrC)}) showed a significant correlation with secondary OC (SOC) in autumn (R =
10 0.90, $p < 0.05$) and winter (R = 0.67, $p < 0.05$). Furthermore, the correlation between FV<sub>S(WSBrc+WI-
11 MSBrC)</sub> and EC in each season was insignificant. Such relations suggest that the secondary
12 formation processes should have been played an important role in controlling the loadings of BrC
13 in autumn and winter as well. A good correlation between FV and Abs₃₆₅ of both WSBrc and WI-
14 MSBrC was found in all seasons except winter, which indicates that most light-absorbing materials
15 would also have significant fluorescence characteristics.

16 The relative contents of different chromophores in different polar extracts depend on their
17 sources and varied significantly. The results showed that the NFVs of WSBrc were lower than
18 those the WI-MSBrC and were different from season to season in Tianjin (Fig. 7). Recently, it has
19 been reported that the aerosols derived from biomass burning and coal combustion exhibit the
20 highest NFV values, while SOA show the lowest NFV values (Chen et al., 2020). NFV in all
21 samples studied in Tianjin during 2018–2019 was very similar to that of primary emissions and
22 higher than that of secondary aerosols. Such result reveal that the fluorophores in the Tianjin PM_{2.5}
23 might mainly be derived from a primary combustion sources as well. In addition, the NFVs of the
24 Tianjin PM_{2.5} were higher in winter than in summer, which is likely and can be attributed to the
25 photolysis of chromophores in summer. In addition, NFV of WI-MSBrC was much higher than
26 that in WSBrc, which indicate that fluorescence contribution of fluorophores was abundant in WI-
27 MSBrC than in the WSBrc.



28
29 **Figure 7.** The normalized fluorescence volumes (NFVs) of the WSBrc and WI-MSBrC of PM_{2.5}
30 from Tianjin, North China.

4. Summary and Conclusions

This study presents the temporal variations in light absorption and fluorescence properties of water-soluble BrC (WSBrC) and the water-insoluble but MeOH-soluble BrC (WI-MSBrC) in PM_{2.5} collected from Tianjin, North China during July 5, 2018 – July 5, 2019. Light absorption properties of WSBrC and WI-MSBrC in Tianjin were investigated and found to be distinct from season to season, which was lower in spring and summer, compared with that in autumn and winter. The AAE of WI-MSBrC was comparable with that of WSBrC. The mass absorption efficiency of WSBrC and WI-MSBrC (MAE₃₆₅) exhibited distinct seasonal variations, which was higher in winter and lower in summer and autumn. Biologically derived or secondary BrC and/or its photobleaching might be the reasons for the lower MAE₃₆₅ values in summer and autumn. The light absorption of both WSBrC and WI-MSBrC in the range of 300–400 nm to that in the whole range (300–700 nm) was ~40%, indicating that BrC in the UV-Vis range plays an important role in climate warming. In addition, based on PARAFAC analysis model, EEM data were comprehensively analyzed to identify the types and abundance of different fluorophores, and obtained three types of the fluorophores: low-oxygenated HULIS, high-oxygenated HULIS and protein-like compound (PLOM). The correlation between BrC optical properties and aerosol chemical composition indicated that biomass burning, and fossil fuel (mainly coal) combustion significantly contributed to BrC content in winter, while primary biological emission and subsequent aging significantly contributed to the BrC content in summer. These results illustrated the light absorption properties of BrC in metropolis aerosols and emphasized its significant contribution to radiative forcing.

Declaration of competing interest

The authors declare no competing interest in this paper.

Data Availability Statement

The data used in this study can be found online at <https://doi.org/10.5281/zenodo.7316371> (Dong et al., 2022), and at <https://doi.org/10.5281/zenodo.5140861> (Dong et al., 2021).

Supplement.

The supplement related to this article is available online at:

Acknowledgments

This work was supported in part by National Natural Science Foundation of China (Grant No. 41775120 and 42277090) & National Key Research and Development Plan (Grant No. 2017YFC0212700), China. The author also thanks to Mr. Yunting Xiao's help for writing a code to calculate the SFE.

Author contribution

ZD and CMP conceptualized this study. ZD and PL conducted the sampling. ZD conducted the

1 chemical analyses, interpreted the data and wrote the manuscript. CMP supervised the research
2 and acquired the funding for this study. XZ, ZXY and ZXJ administrated the project. CMP, ZX,
3 DJ, PF and CQL contributed in discussing the results and review and editing the manuscript.

4 **References**

- 5 Andreae, M. O. and Gelencsér, A.: Black carbon or brown carbon? The nature of light-absorbing carbonaceous
6 aerosols, *Atmospheric Chemistry and Physics*, 6, 3131–3148, www.atmos-chem-phys.net/6/3131/2006/, 2006.
- 7 Baduel, C., Voisin, D., and Jaffrezo, J. L.: Comparison of analytical methods for Humic Like Substances (HULIS)
8 measurements in atmospheric particles, *Atmospheric Chemistry and Physics*, 9, 5949–5962, 10.5194/acp-9-5949-
9 2009, 2009.
- 10 Birdwell, J. E. and Engel, A. S.: Characterization of dissolved organic matter in cave and spring waters using UV-
11 Vis absorbance and fluorescence spectroscopy, *Org Geochem*, 41, 270–280, 10.1016/j.orggeochem.2009.11.002,
12 2010.
- 13 Bond, T. C. and Bergstrom, R. W.: Light absorption by carbonaceous particles: An investigative review, *Aerosol*
14 *Science and Technology*, 40, 27–67, 10.1080/02786820500421521, 2006.
- 15 Brown, H., Liu, X., Pokhrel, R., Murphy, S., Lu, Z., Saleh, R., Mielonen, T., Kokkola, H., Bergman, T., Myhre, G.,
16 Skeie, R. B., Watson-Paris, D., Stier, P., Johnson, B., Bellouin, N., Schulz, M., Vakkari, V., Beukes, J. P., van Zyl,
17 P. G., Liu, S., and Chand, D.: Biomass burning aerosols in most climate models are too absorbing, *Nature*
18 *Communications*, 12, 277, 10.1038/s41467-020-20482-9, 2021.
- 19 Cao, T., Li, M., Xu, C., Song, J., Fan, X., Li, J., Jia, W., and Peng, P.: Technical note: Identification of chemical
20 composition and source of fluorescent components in atmospheric water-soluble brown carbon by excitation-
21 emission matrix with parallel factor analysis: Potential limitation and application, *Atmospheric Chemistry and*
22 *Physics Discussions*, 2022, 1–41, 10.5194/acp-2022-676, 2022.
- 23 Chen, Q., Fumikazu, I., Hayato, H., Daichi, A., and Michihiro, M.: Chemical structural characteristics of HULIS
24 and other fractionated organic matter in urban aerosols: Results from mass spectral and FT-IR analysis,
25 *Environmental Science & Technology*, 50, 1721–1730, 10.1021/acs.est.5b05277, 2016a.
- 26 Chen, Q., Mu, Z., Song, W., Wang, Y., Yang, Z., Zhang, L., and Zhang, Y.-L.: Size-resolved characterization of the
27 chromophores in atmospheric particulate matter from a typical coal-burning city in China, *Journal of Geophysical*
28 *Research: Atmospheres*, 124, 10546–10563, <https://doi.org/10.1029/2019JD031149>, 2019.
- 29 Chen, Q., Li, J., Hua, X., Jiang, X., Mu, Z., Wang, M., Wang, J., Shan, M., Yang, X., Fan, X., Song, J., Wang, Y.,
30 Guan, D., and Du, L.: Identification of species and sources of atmospheric chromophores by fluorescence excitation-
31 emission matrix with parallel factor analysis, *Science of the Total Environment*, 718, 137322,
32 10.1016/j.scitotenv.2020.137322, 2020.
- 33 Chen, Q., Miyazaki, Y., Kawamura, K., Matsumoto, K., Coburn, S., Volkamer, R., Iwamoto, Y., Kagami, S., Deng,
34 Y., Ogawa, S., Ramasamy, S., Kato, S., Ida, A., Kajii, Y., and Mochida, M.: Characterization of chromophoric
35 water-soluble organic matter in urban, forest, and marine aerosols by HR-ToF-AMS analysis and excitation-
36 emission matrix spectroscopy, *Environmental Science & Technology*, 50, 10351–10360, 10.1021/acs.est.6b01643,
37 2016b.
- 38 Chen, Q. C., Ikemori, F., and Mochida, M.: Light Absorption and Excitation-Emission Fluorescence of Urban
39 Organic Aerosol Components and Their Relationship to Chemical Structure, *Environ Sci Technol*, 50, 10859–10868,
40 10.1021/acs.est.6b02541, 2016c.
- 41 Choudhary, V., Rajput, P., and Gupta, T.: Absorption properties and forcing efficiency of light-absorbing water-
42 soluble organic aerosols: Seasonal and spatial variability, *Environ Pollut*, 272, ARTN 115932
43 10.1016/j.envpol.2020.115932, 2021.
- 44 Coble, P. G.: Marine optical biogeochemistry: The chemistry of ocean color, *Chem Rev*, 107, 402–418,
45 10.1021/cr050350+, 2007.
- 46 Corbin, J. C., Czech, H., Massabò, D., de Mongeot, F. B., Jakobi, G., Liu, F., Lobo, P., Mennucci, C., Mensah, A.
47 A., Orasche, J., Pieber, S. M., Prévôt, A. S. H., Stengel, B., Tay, L. L., Zanatta, M., Zimmermann, R., El Haddad, I.,
48 and Gysel, M.: Infrared-absorbing carbonaceous tar can dominate light absorption by marine-engine exhaust, *npj*
49 *Climate and Atmospheric Science*, 2, 12, 10.1038/s41612-019-0069-5, 2019.
- 50 Deng, J., Ma, H., Wang, X., Zhong, S., Zhang, Z., Zhu, J., Fan, Y., Hu, W., Wu, L., Xiaodong, L., Ren, L., Pavuluri,
51 C. M., Pan, X., Sun, Y., Wang, Z., Kawamura, K., and Fu, P.: Measurement Report: Optical properties and sources

1 of water-soluble brown carbon in Tianjin, North China: insights from organic molecular compositions, *Atmospheric*
2 *Chemistry and Physics*, 22, 6449-6470, 10.5194/acp-2021-1045, 2022.

3 Diggs, D. L., Huderson, A. C., Harris, K. L., Myers, J. N., Banks, L. D., Rekhadevi, P. V., Niaz, M. S., and Ramesh,
4 A.: Polycyclic aromatic hydrocarbons and digestive tract cancers: a perspective, *Journal of Environmental Science*
5 *and Health, Part C*, 29, 324-357, 10.1080/10590501.2011.629974, 2011.

6 Dong, Z., Pavuluri, C. M., Xu, Z., Wang, Y., Li, P., Fu, P., and Liu, C. Q.: Measurement report: Chemical
7 components and ¹³C and ¹⁵N isotope ratios of fine aerosols over Tianjin, North China: year-round observations,
8 *Atmospheric Chemistry and Physics*, 23, 2119-2143, 10.5194/acp-23-2119-2023, 2023a.

9 Dong, Z. C., Pavuluri, C. M., Li, P. S., Xu, Z. J., Deng, J. J., Zhao, X. Y., and Zhao, X. M.: Year-round observations
10 of the optical properties of brown carbon in fine aerosols at Tianjin, North China – Data set,
11 <https://doi.org/10.5281/zenodo.7316371>, 2022.

12 Dong, Z. C., Pavuluri, C. M., Xu, Z. J., Wang, Y., Li, P. S., Fu, P. Q., and Liu, C. Q.: Year-round observations of
13 bulk components and ¹³C and ¹⁵N isotope ratios of fine aerosols at Tianjin, North China – Data set,
14 <https://doi.org/10.5281/zenodo.5140861>, 2021.

15 Dong, Z. C., Pavuluri, C. M., Xu, Z. J., Wang, Y., Li, P. S., Fu, P. Q., and Liu, C. Q.: Measurement report:
16 Chemical components and
17 C and
18 N isotoperatios of fine aerosols over Tianjin, North China: year-round observations, *Atmos Chem Phys*, 23, 2119-
19 2143, 10.5194/acp-23-2119-2023, 2023b.

20 Fan, X. J., Wei, S. Y., Zhu, M. B., Song, J. Z., and Peng, P. A.: Comprehensive characterization of humic-like
21 substances in smoke PM
22 emitted from the combustion of biomass materials and fossil fuels, *Atmos Chem Phys*, 16, 13321-13340,
23 10.5194/acp-16-13321-2016, 2016.

24 Feng, Y., Ramanathan, V., and Kotamarthi, V. R.: Brown carbon: a significant atmospheric absorber of solar
25 radiation?, *Atmospheric Chemistry and Physics Discussions*, 10.5194/acpd-13-2795-2013, 2013.

26 Gao yan and Zhang, y.: Formation and photochemical investigation of brown carbon by hydroxyacetone reactions
27 with glycine and ammonium sulfate, *Royal Society of Chemistry Advances*, 8, 20719-20725,
28 10.1039/C8RA02019A, 2018.

29 Gu, Q. and Kenny, J. E.: Improvement of inner filter effect correction based on determination of effective geometric
30 parameters using a conventional fluorimeter, *Analytical Chemistry*, 81, 420-426, 10.1021/ac801676j, 2009.

31 Hecobian, A., Zhang, X., Zheng, M., Frank, N., Edgerton, E. S., and Weber, R. J.: Water-Soluble Organic Aerosol
32 material and the light-absorption characteristics of aqueous extracts measured over the Southeastern United States,
33 *Atmos Chem Phys*, 10, 5965-5977, 10.5194/acp-10-5965-2010, 2010.

34 Hems, R. F., Schnitzler, E. G., Liu-Kang, C., Cappa, C. D., and Abbatt, J. P. D.: Aging of atmospheric brown carbon
35 aerosol, *ACS Earth and Space Chemistry*, 5, 722-748, 10.1021/acsearthspacechem.0c00346, 2021.

36 Hoffer, A., Gelencsér, A., Guyon, P., Kiss, G., Schmid, O., Frank, G. P., Artaxo, P., and Andreae, M. O.: Optical
37 properties of humic-like substances (HULIS) in biomass-burning aerosols, *Atmospheric Chemistry and Physics*, 6,
38 3563-3570, 10.5194/acp-6-3563-2006, 2006.

39 Huang, R. J., Yang, L., Cao, J., Chen, Y., Chen, Q., Li, Y., Duan, J., Zhu, C., Dai, W., Wang, K., Lin, C., Ni, H.,
40 Corbin, J. C., Wu, Y., Zhang, R., Tie, X., Hoffmann, T., O'Dowd, C., and Dusek, U.: Brown carbon aerosol in urban
41 Xi'an, Northwest China: The composition and light absorption properties, *Environmental Science & Technology*,
42 52, 6825-6833, 10.1021/acs.est.8b02386, 2018.

43 Huang, R. J., Yang, L., Shen, J., Yuan, W., Gong, Y., Guo, J., Cao, W., Duan, J., Ni, H., Zhu, C., Dai, W., Li, Y.,
44 Chen, Y., Chen, Q., Wu, Y., Zhang, R., Dusek, U., O'Dowd, C., and Hoffmann, T.: Water-insoluble organics
45 dominate brown carbon in wintertime urban aerosol of China: Chemical characteristics and optical properties,
46 *Environmental Science & Technology*, 54, 7836-7847, 10.1021/acs.est.0c01149, 2020.

47 Jo, D. S., Park, R. J., Lee, S., Kim, S. W., and Zhang, X.: A global simulation of brown carbon: implications for
48 photochemistry and direct radiative effect, *Atmospheric Chemistry and Physics*, 16, 3413-3432, 10.5194/acp-16-
49 3413-2016, 2016.

50 Kasthuriarachchi, N. Y., Rivellini, L.-H., Chen, X., Li, Y. J., and Lee, A. K. Y.: Effect of relative humidity on
51 secondary brown carbon formation in aqueous droplets, *Environmental Science & Technology*, 54, 13207-13216,
52 10.1021/acs.est.0c01239, 2020.

53 Lack, D. A., Bahreni, R., Langridge, J. M., Gilman, J. B., and Middlebrook, A. M.: Brown carbon absorption linked
54 to organic mass tracers in biomass burning particles, *Atmospheric Chemistry and Physics*, 13, 2415-2422,
55 10.5194/acp-13-2415-2013, 2013.

1 Laskin, A., Laskin, J., and Nizkorodov, S. A.: Chemistry of atmospheric brown carbon, *Chemical Reviews*, 115,
2 4335-4382, 10.1021/cr5006167, 2015a.

3 Laskin, A., Laskin, J., and Nizkorodov, S. A.: Chemistry of Atmospheric Brown Carbon, *Chem Rev*, 115, 4335-
4 4382, 10.1021/cr5006167, 2015b.

5 Lawaetz, A. J. and Stedmon, C. A.: Fluorescence intensity calibration using the Raman scatter peak of water,
6 *Applied Spectroscopy*, 63, 936-940, 10.1366/000370209788964548, 2009.

7 Lee, H. J., Laskin, A., Laskin, J., and Nizkorodov, S. A.: Excitation-Emission Spectra and Fluorescence Quantum
8 Yields for Fresh and Aged Biogenic Secondary Organic Aerosols, *Environ Sci Technol*, 47, 5763-5770,
9 10.1021/es400644c, 2013.

10 Lesworth, T., Baker, A. R., and Jickells, T.: Aerosol organic nitrogen over the remote Atlantic Ocean, *Atmospheric*
11 *Environment*, 44, 1887-1893, <https://doi.org/10.1016/j.atmosenv.2010.02.021>, 2010.

12 Li, C., He, Q., Hettiyadura, A. P. S., Käfer, U., Shmul, G., Meidan, D., Zimmermann, R., Brown, S. S., George, C.,
13 Laskin, A., and Rudich, Y.: Formation of secondary brown carbon in biomass burning aerosol proxies through NO₃
14 radical reactions, *Environmental Science & Technology*, 54, 1395-1405, 10.1021/acs.est.9b05641, 2020a.

15 Li, J., Zhang, Q., Wang, G., Li, J., Wu, C., Liu, L., Wang, J., Jiang, W., Li, L., Ho, K. F., and Cao, J.: Optical
16 properties and molecular compositions of water-soluble and water-insoluble brown carbon (BrC) aerosols in
17 northwest China, *Atmospheric Chemistry and Physics*, 20, 4889-4904, 10.5194/acp-20-4889-2020, 2020b.

18 Li, S., Zhu, M., Yang, W. Q., Tang, M. J., Huang, X. L., Yu, Y. G., Fang, H., Yu, X., Yu, Q. Q., Fu, X. X., Song,
19 W., Zhang, Y. L., Bi, X. H., and Wang, X. M.: Filter-based measurement of light absorption by brown carbon in
20 PM_{2.5} in a megacity in South China, *Science of the Total Environment*, 633, 1360-1369,
21 10.1016/j.scitotenv.2018.03.235, 2018.

22 Li, X., Fu, P., Tripathee, L., Yan, F., Hu, Z., Yu, F., Chen, Q., Li, J., Chen, Q., Cao, J., and Kang, S.: Molecular
23 compositions, optical properties, and implications of dissolved brown carbon in snow/ice on the Tibetan Plateau
24 glaciers, *Environment International*, 164, 107276, <https://doi.org/10.1016/j.envint.2022.107276>, 2022.

25 Liakakou, E., Kaskaoutis, D. G., Grivas, G., Stavroulas, I., Tsagkaraki, M., Paraskevopoulou, D., Bougiatioti, A.,
26 Dumka, U. C., Gerasopoulos, E., and Mihalopoulos, N.: Long-term brown carbon spectral characteristics in a
27 Mediterranean city (Athens), *Sci Total Environ*, 708, 135019, 10.1016/j.scitotenv.2019.135019, 2020.

28 Lin, G., Penner, J. E., Flanner, M. G., Sillman, S., Xu, L., and Zhou, C.: Radiative forcing of organic aerosol in the
29 atmosphere and on snow: Effects of SOA and brown carbon, *Journal of Geophysical Research: Atmospheres*, 119,
30 7453-7476, 10.1002/2013jd021186, 2014.

31 Lin, P., Bluvshtein, N., Rudich, Y., Nizkorodov, S. A., Laskin, J., and Laskin, A.: Molecular Chemistry of
32 Atmospheric Brown Carbon Inferred from a Nationwide Biomass Burning Event, *Environ Sci Technol*, 51, 11561-
33 11570, 10.1021/acs.est.7b02276, 2017.

34 Liu, J., Bergin, M., Guo, H., King, L., Kotra, N., Edgerton, E., and Weber, R. J.: Size-resolved measurements of
35 brown carbon in water and methanol extracts and estimates of their contribution to ambient fine-particle light
36 absorption, *Atmospheric Chemistry and Physics*, 13, 12389-12404, 10.5194/acp-13-12389-2013, 2013.

37 McKnight, D. M., Boyer, E. W., Westerhoff, P. K., Doran, P. T., Kulbe, T., and Andersen, D. T.:
38 Spectrofluorometric characterization of dissolved organic matter for indication of precursor organic material and
39 aromaticity, *Limnol Oceanogr*, 46, 38-48, DOI 10.4319/lo.2001.46.1.0038, 2001.

40 Murphy, K. R., Stedmon, C. A., Graeber, D., and Bro, R.: Fluorescence spectroscopy and multi-way techniques.
41 PARAFAC, *Anal Methods-Uk*, 5, 6557-6566, 10.1039/c3ay41160e, 2013.

42 Park, R. J., Kim, M. J., Jeong, J. I., Youn, D., and Kim, S.: A contribution of brown carbon aerosol to the aerosol
43 light absorption and its radiative forcing in East Asia, *Atmospheric Environment*, 44, 1414-1421,
44 10.1016/j.atmosenv.2010.01.042, 2010.

45 Peters, S., Talaska, G., Jonsson, B. A., Kromhout, H., and Vermeulen, R.: Polycyclic aromatic hydrocarbon
46 exposure, urinary mutagenicity, and DNA adducts in rubber manufacturing workers, *Cancer Epidemiol Biomarkers*
47 *Prev*, 17, 1452-1459, 10.1158/1055-9965.EPI-07-2777, 2008.

48 Qin, J., Zhang, L., Zhou, X., Duan, J., Mu, S., Xiao, K., Hu, J., and Tan, J.: Fluorescence fingerprinting properties
49 for exploring water-soluble organic compounds in PM_{2.5} in an industrial city of northwest China, *Atmospheric*
50 *Environment*, 184, 203-211, <https://doi.org/10.1016/j.atmosenv.2018.04.049>, 2018.

51 Rizzo, L. V., Correia, A. L., Artaxo, P., Procópio, A. S., and Andreae, M. O.: Spectral dependence of aerosol light
52 absorption over the Amazon Basin, *Atmospheric Chemistry and Physics*, 11, 8899-8912, 10.5194/acp-11-8899-
53 2011, 2011.

54 Rizzo, L. V., Artaxo, P., Müller, T., Wiedensohler, A., Paixão, M., Cirino, G. G., Arana, A., Swietlicki, E., Roldin,
55 P., Fors, E. O., Wiedemann, K. T., Leal, L. S. M., and Kulmala, M.: Long term measurements of aerosol optical

1 properties at a primary forest site in Amazonia, *Atmos. Chem. Phys.*, 13, 2391-2413, 10.5194/acp-13-2391-2013,
2 2013.

3 Shamjad, P. M., Tripathi, S. N., Thamban, N. M., and Vreeland, H.: Refractive Index and Absorption Attribution of
4 Highly Absorbing Brown Carbon Aerosols from an Urban Indian City-Kanpur, *Sci Rep-Uk*, 6, 10.1038/srep37735,
5 2016.

6 Shetty, N. J., Pandey, A., Baker, S., Hao, W. M., and Chakrabarty, R. K.: Measuring light absorption by freshly
7 emitted organic aerosols: optical artifacts in traditional solvent-extraction-based methods, *Atmos Chem Phys*, 19,
8 8817-8830, 10.5194/acp-19-8817-2019, 2019.

9 Sun, J., Zhi, G., Hitznerberger, R., Chen, Y., Tian, C., Zhang, Y., Feng, Y., Cheng, M., Zhang, Y., Cai, J., Chen, F.,
10 Qiu, Y., Jiang, Z., Li, J., Zhang, G., and Mo, Y.: Emission factors and light absorption properties of brown carbon
11 from household coal combustion in China, *Atmos. Chem. Phys.*, 17, 4769-4780, 10.5194/acp-17-4769-2017, 2017.

12 Tang, J., Li, J., Mo, Y., Safaei Khorram, M., Chen, Y., Tang, J., Zhang, Y., Song, J., and Zhang, G.: Light
13 absorption and emissions inventory of humic-like substances from simulated rainforest biomass burning in
14 Southeast Asia, *Environmental Pollution*, 262, 114266, <https://doi.org/10.1016/j.envpol.2020.114266>, 2020.

15 Wang, D., Shen, Z., Zhang, Q., Lei, Y., Zhang, T., Huang, S., Sun, J., Xu, H., and Cao, J.: Winter brown carbon
16 over six of China's megacities: light absorption, molecular characterization, and improved source apportionment
17 revealed by multilayer perceptron neural network, *Atmospheric Chemistry and Physics*, 22, 14893-14904,
18 10.5194/acp-22-14893-2022, 2022a.

19 Wang, Q. Q., Zhou, Y. Y., Ma, N., Zhu, Y., Zhao, X. C., Zhu, S. W., Tao, J. C., Hong, J., Wu, W. J., Cheng, Y. F.,
20 and Su, H.: Review of brown carbon aerosols in China: Pollution level, optical properties, and emissions, *Journal of*
21 *Geophysical Research: Atmospheres*, 127, 10.1029/2021JD035473, 2022b.

22 Wang, Y., Pavuluri, C. M., Fu, P., Li, P., Dong, Z., Xu, Z., Ren, H., Fan, Y., Li, L., Zhang, Y.-L., and Liu, C.-Q.:
23 Characterization of Secondary Organic Aerosol Tracers over Tianjin, North China during Summer to Autumn, *ACS*
24 *Earth and Space Chemistry*, 3, 2339-2352, 10.1021/acsearthspacechem.9b00170, 2019.

25 Wen, H., Zhou, Y., Xu, X., Wang, T., Chen, Q., Chen, Q., Li, W., Wang, Z., Huang, Z., Zhou, T., Shi, J., Bi, J., Ji,
26 M., and Wang, X.: Water-soluble brown carbon in atmospheric aerosols along the transport pathway of Asian dust:
27 Optical properties, chemical compositions, and potential sources, *Science of the Total Environment*, 789, 147971,
28 10.1016/j.scitotenv.2021.147971, 2021.

29 Wu, G., Fu, P., Ram, K., Song, J., Chen, Q., Kawamura, K., Wan, X., Kang, S., Wang, X., Laskin, A., and Cong, Z.:
30 Fluorescence characteristics of water-soluble organic carbon in atmospheric aerosol, *Environmental Pollution*, 268,
31 115906, 10.1016/j.envpol.2020.115906, 2021a.

32 Wu, G. M., Fu, P. Q., Ram, K., Song, J. Z., Chen, Q. C., Kawamura, K., Wan, X., Kang, S. C., Wang, X. P., Laskin,
33 A., and Cong, Z. Y.: Fluorescence characteristics of water-soluble organic carbon in atmospheric aerosol, *Environ*
34 *Pollut*, 268, ARTN 115906
35 10.1016/j.envpol.2020.115906, 2021b.

36 Xie, X., Chen, Y., Nie, D., Liu, Y., Liu, Y., Lei, R., Zhao, X., Li, H., and Ge, X.: Light-absorbing and fluorescent
37 properties of atmospheric brown carbon: A case study in Nanjing, China, *Chemosphere*, 251, 126350,
38 10.1016/j.chemosphere.2020.126350, 2020.

39 Yan, J., Wang, X., Gong, P., Wang, C., and Cong, Z.: Review of brown carbon aerosols: Recent progress and
40 perspectives, *Sci Total Environ*, 634, 1475-1485, 10.1016/j.scitotenv.2018.04.083, 2018.

41 Yu, H., Liang, H., Qu, F., Han, Z. S., Shao, S., Chang, H., and Li, G.: Impact of dataset diversity on accuracy and
42 sensitivity of parallel factor analysis model of dissolved organic matter fluorescence excitation-emission matrix,
43 *Scientific Reports*, 5, 10207, 10.1038/srep10207, 2015.

44 Yue, S., Zhu, J., Chen, S., Xie, Q., Li, W., Li, L., Ren, H., Sihui, S., Ping, L., Ma, H., Fan, Y., Cheng, B., Wu, L.,
45 Deng, J., Hu, W., Ren, L., Lianfang, W., Zhao, W., Tian, Y., and Fu, P.: Brown carbon from biomass burning
46 imposes strong circum-Arctic warming, *One Earth*, 5, 293-304, 10.1016/j.oneear.2022.02.006, 2022.

47 Yue, S. Y., Bikkina, S., Gao, M., Barrie, L., Kawamura, K., and Fu, P. Q.: Sources and Radiative Absorption of
48 Water-Soluble Brown Carbon in the High Arctic Atmosphere, *Geophys Res Lett*, 46, 14881-14891,
49 10.1029/2019gl085318, 2019.

50 Zhan, Y., Li, J., Tsona, N. T., Chen, B., Yan, C., George, C., and Du, L.: Seasonal variation of water-soluble brown
51 carbon in Qingdao, China: Impacts from marine and terrestrial emissions, *Environmental Research*, 212, 113144,
52 <https://doi.org/10.1016/j.envres.2022.113144>, 2022.

53 Zhang, Q., Jimenez, J. L., Canagaratna, M. R., Ulbrich, I. M., Ng, N. L., Worsnop, D. R., and Sun, Y.:
54 Understanding atmospheric organic aerosols via factor analysis of aerosol mass spectrometry: a review, *Analytical*
55 *Chemistry and Bioanalytical Chemistry*, 401, 3045-3067, 10.1007/s00216-011-5355-y, 2011.

1 Zhang, Q., Shen, Z., Zhang, T., Kong, S., Lei, Y., Wang, Q., Tao, J., Zhang, R., Wei, P., Wei, C., Cui, S., Cheng, T.,
2 Ho, S. S. H., Li, Z., Xu, H., and Cao, J.: Spatial distribution and sources of winter black carbon and brown carbon in
3 six Chinese megacities, *Science of The Total Environment*, 762, 143075,
4 <https://doi.org/10.1016/j.scitotenv.2020.143075>, 2021.

5 Zhong, M. and Jang, M.: Light absorption coefficient measurement of SOA using a UV–Visible spectrometer
6 connected with an integrating sphere, *Atmospheric Environment*, 45, 4263-4271, 10.1016/j.atmosenv.2011.04.082,
7 2011.

8 Zhu, C. S., Cao, J. J., Huang, R. J., Shen, Z. X., Wang, Q. Y., and Zhang, N. N.: Light absorption properties of
9 brown carbon over the southeastern Tibetan Plateau, *Science of the Total Environment*, 625, 246-251,
10 10.1016/j.scitotenv.2017.12.183, 2018.

11